Real-Time Control of a Class of Kinematically Redundant Industrial Machines

by

Navtej Singh

A Thesis

Submitted to the Faculty of Graduate Studies

in Partial Fulfillment of the Requirements

for the Degree of

Master of Science

Department of Mechanical & Industrial Engineering

University of Manitoba

Winnipeg, Manitoba, Canada

ISBN 0-315-98984-X

Name NAVTEJ SINGH

Dissertation Abstracts International is arranged by broad, general subject categories. Please select the one subject which most nearly describes the content of your dissertation. Enter the corresponding four-digit code in the spaces provided.

INDUSTRIAL ENGINEERING
SUBJECT TERM

0546
SUBJECT CODE

U·M·I

Subject Categories

THE HUMANITIES AND SOCIAL SCIENCES

COMMUNICATIONS AND THE ARTS
Architecture 0729
Art History 0377
Cinema 0900
Dance 0378
Fine Arts 0357
Information Science 0723
Journalism 0391
Library Science 0399
Mass Communications 0708
Music 0413
Speech Communication 0459
Theater 0465

EDUCATION
General 0515
Administration 0514
Adult and Continuing 0516
Agricultural 0517
Art 0273
Bilingual and Multicultural 0282
Business 0688
Community College 0275
Curriculum and Instruction 0727
Early Childhood 0518
Elementary 0524
Finance 0277
Guidance and Counseling 0519
Health 0680
Higher 0745
History of 0520
Home Economics 0278
Industrial 0521
Language and Literature 0279
Mathematics 0280
Music 0522
Philosophy of 0998
Physical 0523

Psychology 0525
Reading 0535
Religious 0527
Sciences 0714
Secondary 0533
Social Sciences 0534
Sociology of 0340
Special 0529
Teacher Training 0530
Technology 0710
Tests and Measurements 0288
Vocational 0747

LANGUAGE, LITERATURE AND LINGUISTICS
Language
- General 0679
- Ancient 0289
- Linguistics 0290
- Modern 0291

Literature
- General 0401
- Classical 0294
- Comparative 0295
- Medieval 0297
- Modern 0298
- African 0316
- American 0591
- Asian 0305
- Canadian (English) 0352
- Canadian (French) 0355
- English 0593
- Germanic 0311
- Latin American 0312
- Middle Eastern 0315
- Romance 0313
- Slavic and East European 0314

PHILOSOPHY, RELIGION AND THEOLOGY
Philosophy 0422
Religion
- General 0318
- Biblical Studies 0321
- Clergy 0319
- History of 0320
- Philosophy of 0322

Theology 0469

SOCIAL SCIENCES
American Studies 0323
Anthropology
- Archaeology 0324
- Cultural 0326
- Physical 0327

Business Administration
- General 0310
- Accounting 0272
- Banking 0770
- Management 0454
- Marketing 0338

Canadian Studies 0385
Economics
- General 0501
- Agricultural 0503
- Commerce-Business 0505
- Finance 0508
- History 0509
- Labor 0510
- Theory 0511

Folklore 0358
Geography 0366
Gerontology 0351
History
- General 0578
- Ancient 0579
- Medieval 0581
- Modern 0582
- Black 0328
- African 0331
- Asia, Australia and Oceania 0332
- Canadian 0334
- European 0335
- Latin American 0336
- Middle Eastern 0333
- United States 0337

History of Science 0585
Law 0398
Political Science
- General 0615
- International Law and Relations 0616
- Public Administration 0617

Recreation 0814
Social Work 0452
Sociology
- General 0626
- Criminology and Penology 0627
- Demography 0938
- Ethnic and Racial Studies 0631
- Individual and Family Studies 0628
- Industrial and Labor Relations 0629
- Public and Social Welfare 0630
- Social Structure and Development 0700
- Theory and Methods 0344

Transportation 0709
Urban and Regional Planning 0999
Women's Studies 0453

THE SCIENCES AND ENGINEERING

BIOLOGICAL SCIENCES
Agriculture
- General 0473
- Agronomy 0285
- Animal Culture and Nutrition 0475
- Animal Pathology 0476
- Food Science and Technology 0359
- Forestry and Wildlife 0478
- Plant Culture 0479
- Plant Pathology 0480
- Plant Physiology 0817
- Range Management 0777
- Wood Technology 0746

Biology
- General 0306
- Anatomy 0287
- Biostatistics 0308
- Botany 0309
- Cell 0379
- Ecology 0329
- Entomology 0353
- Genetics 0369
- Limnology 0793
- Microbiology 0410
- Molecular 0307
- Neuroscience 0317
- Oceanography 0416
- Physiology 0433
- Radiation 0821
- Veterinary Science 0778
- Zoology 0472

Biophysics
- General 0786
- Medical 0760

EARTH SCIENCES
Biogeochemistry 0425
Geochemistry 0996
Geodesy 0370
Geology 0372
Geophysics 0373
Hydrology 0388
Mineralogy 0411
Paleobotany 0345
Paleoecology 0426
Paleontology 0418
Paleozoology 0985
Palynology 0427
Physical Geography 0368
Physical Oceanography 0415

HEALTH AND ENVIRONMENTAL SCIENCES
Environmental Sciences 0768
Health Sciences
- General 0566
- Audiology 0300
- Chemotherapy 0992
- Dentistry 0567
- Education 0350
- Hospital Management 0769
- Human Development 0758
- Immunology 0982
- Medicine and Surgery 0564
- Mental Health 0347
- Nursing 0569
- Nutrition 0570
- Obstetrics and Gynecology 0380
- Occupational Health and Therapy 0354
- Ophthalmology 0381
- Pathology 0571
- Pharmacology 0419
- Pharmacy 0572
- Physical Therapy 0382
- Public Health 0573
- Radiology 0574
- Recreation 0575
- Speech Pathology 0460
- Toxicology 0383

Home Economics 0386

PHYSICAL SCIENCES
Pure Sciences
Chemistry
- General 0485
- Agricultural 0749
- Analytical 0486
- Biochemistry 0487
- Inorganic 0488
- Nuclear 0738
- Organic 0490
- Pharmaceutical 0491
- Physical 0494
- Polymer 0495
- Radiation 0754

Mathematics 0405
Physics
- General 0605
- Acoustics 0986
- Astronomy and Astrophysics 0606
- Atmospheric Science 0608
- Atomic 0748
- Electronics and Electricity 0607
- Elementary Particles and High Energy 0798
- Fluid and Plasma 0759
- Molecular 0609
- Nuclear 0610
- Optics 0752
- Radiation 0756
- Solid State 0611

Statistics 0463

Applied Sciences
Applied Mechanics 0346
Computer Science 0984
Engineering
- General 0537
- Aerospace 0538
- Agricultural 0539
- Automotive 0540
- Biomedical 0541
- Chemical 0542
- Civil 0543
- Electronics and Electrical 0544
- Heat and Thermodynamics 0348
- Hydraulic 0545
- Industrial 0546
- Marine 0547
- Materials Science 0794
- Mechanical 0548
- Metallurgy 0743
- Mining 0551
- Nuclear 0552
- Packaging 0549
- Petroleum 0765
- Sanitary and Municipal 0554
- System Science 0790

Geotechnology 0428
Operations Research 0796
Plastics Technology 0795
Textile Technology 0994

PSYCHOLOGY
General 0621
Behavioral 0384
Clinical 0622
Developmental 0620
Experimental 0623
Industrial 0624
Personality 0625
Physiological 0989
Psychobiology 0349
Psychometrics 0632
Social 0451

REAL-TIME CONTROL OF A CLASS OF KINEMATICALLY REDUNDANT INDUSTRIAL MACHINES

BY

NAVTEJ SINGH

A Thesis submitted to the Faculty of Graduate Studies of the University of Manitoba in partial fulfillment of the requirements of the degree of

MASTER OF SCIENCE

I hereby declare that I am the sole author of this thesis.

I authorize the University of Manitoba to lend this thesis to other institutions or individuals for the purpose of scholarly research.

Navtej Singh

I further authorize the University of Manitoba to reproduce this thesis by photocopying or by other means, in total or in part, at the request of other institutions or individuals for the purpose of scholarly research.

Navtej Singh

Abstract

This thesis investigates the formulation of the inverse kinematic solution to a class of heavy-duty hydraulic redundant manipulators. A method is presented which utilizes the redundancy to avoid the joint limits, by minimizing a new performance criterion. The proposed performance criterion which is a hyperbolic function of the joint distances from their mid-range, is shown to be advantageous over similar criteria developed by others. Both the joint limit avoidance capability and the smoothness of the resulting joint velocities can be adjusted by the appropriate choice of the parameters introduced in the criterion. Additionally, the criterion includes weight factors to restrict the relative mobility of selected joints.

The application of this work is directed towards heavy-duty mobile equipment used in primary industries. The general goal is to replace the conventional multi-lever (joint-mode) control of these machines with a convenient single-joystick (coordinated-motion) control. With this goal in mind the method is further improved to avoid the bounds on joints while utilizing the maximum power available. Efficient joint motions are determined by incorporating both the required task and dynamic constraints, i.e., end-effector desired speed and loading.

An efficient gradient projection optimization technique is adopted for the numerical solution. The technique is fast and allows real-time applications. The effectiveness of the scheme is demonstrated through computer simulations of a Kyser Spyder excavator machine with one degree of redundancy. Comparison of simulation results with available experimental data are also conducted which indicates that the developed scheme can produce joint trajectories similar to what an experienced operator produces in a conventional joint-mode control.

Acknowledgements

I would like to thank my supervisors, Dr. S. Balakrishnan and Dr. N. Sepehri for their guidance and encouragement through the course of this thesis. Their patience and time are sincerely appreciated.

I must express my special gratitude to Mr. H. Zghal (Department of Mechanical & Industrial Engineering) whose help and contribution in the initial stages of this study made the completion of this Thesis possible.

The time and advice given by the members of my thesis committee, Dr. D. Strong and Dr. W. Pedrycz are also greatly appreciated.

Finally, I wish to thank my family and friends for their patience and understanding during the preparation of this thesis. In particular, I extend my deepest gratitude to my wife Jagdip and to my parents for their encouragement and tolerance throughout my graduate studies.

TABLE OF CONTENTS

CHAPTER PAGE

CHAPTER PAGE

LIST OF FIGURES

FIGURE **PAGE**

FIGURE **PAGE**

LIST OF TABLES

TABLE **PAGE**

Nomenclature

$\dot{\mathbf{x}}$	End-effector velocity vector.
$\dot{\Theta}$	Joint velocity vector.
$\dot{\Theta}_p$	Particular solution.
$\dot{\Theta}_h$	Homogeneous solution (self motion).
$\dot{\Theta}_{MN}$	Minimum-norm least squares solution.
$\mathbf{J}$	Jacobian matrix.
$\mathbf{J}^+$	(Moore-Penrose) generalized Pseudoinverse of the Jacobian $\mathbf{J}$.
$\mathbf{J}^T$	Transpose of the Jacobian $\mathbf{J}$.
$\mathbf{I}$	Identity matrix.
$\mathbf{O}$	Null matrix.
H	Joint limit avoidance criterion.
∇H	Gradient of joint limit avoidance criterion.
$\vec{\boldsymbol{\kappa}}$	Scaling vector.
$\hat{\mathbf{u}}_s$	Unit vector in the direction of the null space of $\mathbf{J}$.
$\mathbf{v_T}$	End-effector velocity vector in Cartesian workspace.
$\mathbf{v_R}$	End-effector velocity vector in Cylindrical workspace.
k	Scaling coefficient.
$\boldsymbol{\alpha}$	Weighing coefficient.
β	Optimization constant.
$\boldsymbol{\phi}$	Configuration factor.
ρ	Achievable joint velocity factor.

CHAPTER 1

INTRODUCTION

1.1 Motivation

Human-operated machinery are being widely used in forestry, mining and construction industries. Excavators and feller bunchers are two examples. These machines are designed to perform heavy-duty tasks such as digging or loading and unloading heavy objects. They have mechanical linkages that utilize high power hydraulic actuators for movement of various joints. The desired task is completed through activation of each link by mechanical levers. For example moving the implement (bucket or the grapple) requires simultaneous coordination of three to four levers. This type of control is normally referred to as "joint-mode control". The speed, dexterity and efficiency of the operation in this mode depends on the experience of the operator.

The control levers in these machines do not translate the intuitive actions initiated by the operator. The operator is hence required to learn the coordinated movement of the control levers for attaining various motions of the implement. This is usually time consuming. Additionally, these machines are operated in unstructured environments with high level of vibrations, noise and heat. The tension and stress for the operator is high, yet he must remain constantly alert in order to accomplish the task, and at the same time, protect his/her own safety as

well as the safety of others. Considering the above aspects, it will be beneficial to automate the operation of these machines.

Functionally the operations of excavators and feller bunchers are very similar to robots and hence offer the possibility of applying the principles of robotics for automating their operation. A successful implementation of this type of technology to these machines will make the operation safe, more productive and less stressful for the operator (Cherchas, 1983). It should be noted however that, although robots prove to be excellent substitutes for human labor in tasks that are hazardous and hostile, they are still deficient in their adaptability to unstructured environments such as those encountered by industrial machines. Recognition of such environments become essential if intelligent online decisions are to be made.

Human operators have the capability to adapt and react to the changes in the surroundings very quickly, whereas today's fully automated robots cannot compete with the speed with which human responds. As a result human cannot be totally removed from the control loop; a situation unlikely to change over the next few decades. Considerable work in the area of human supervisory control has been done by Chavez and Amazeen (1983), Karkkainen and Manninen (1983), Vaha and Halme (1984), and Sheridon (1986).

Recently the University of British Columbia (UBC) in collaboration with Robotic Systems International Research (RSIR) and McMillan Bloadel Research (MBR) implemented a "coordinated-motion control" concept on an instrumented Caterpillar 215B [1] excavator (Lawrence *et al.* 1993). The end-effector of the ma-

[1] Caterpillar 215B is manufactured by Caterpillar Ltd.

chine was controlled by velocity commands arising from a single joystick capable of movement in three directions. The direction of the joystick action was the same as the direction of the motion required at the end-effector. The required joint motions were determined by inverse kinematic procedure and appropriate control signals, were sent to each actuator. This concept which improved the machine operation (Roper 1989) was the first step towards developing a human supervisory control system. The objective of this thesis is to extend this concept further to the class of heavy-duty machines with redundancy. The focus is on developing an appropriate inverse kinematic solution to meet a set of requirements described in the following section.

1.2 Objective and Scope of this Work

In this thesis, an inverse kinematic scheme is developed to utilize the redundancy present in many of the heavy-duty machines. This is expected to enhance the control of these machines. The following requirements are considered during the course of this study.

1. An operator is assumed to be present in the loop and hence the scheme should be able to provide solutions in real-time.

2. Machines of this category are hydraulically actuated. As the piston approaches the limits of the cylinder (referred to as joint limits), the performance of the actuator may present control problems. Therefore, joint limit avoidance should be considered.

3. The comfort of the operator must be considered by generating smooth variation in joint velocities.

4. The scheme should be able to fully utilize the power available at each joint.

The organization of this thesis is as follows. A typical heavy-duty machine with one degree of redundancy is first described in Chapter 2. A general review of coordinated-motion control, as applied to such machines is explained next. Complexity of the inverse kinematic solution for such redundant machines is then discussed. The importance of utilization of redundancy to improve the control is also outlined.

Chapter 3 will discuss the application of the gradient projection optimization technique to solve for inverse kinematics of redundant manipulators for a given performance criterion. The new performance criterion developed during the course of this study is presented and is compared to the performance criteria previously developed by other researchers. A novel scheme that works in conjunction with the gradient optimization technique, to efficiently utilize the coupled power for achieving the highest possible joint velocities, is also presented. The chapter finally outlines the implementation of the algorithm to the class of heavy-duty machines under investigation.

Chapter 4 presents the results of simulation studies conducted using a PC - based simulator, developed as part of this thesis. Conclusions are presented in Chapter 5.

CHAPTER 2

RELEVANT BACKGROUND

A typical heavy-duty industrial machine (a Spyder Kaiser machine) [1] can be best described with reference to Figure 2.1. The machine shown is a mobile four-degree-of-freedom redundant manipulator with an additional movable end-effector, namely the "bucket". The bucket is used to excavate the earth and carry the loads to a drop-off point. It could be substituted by other accessories such as a "grapple" for holding and handling objects, like tree trunks. The motion of the upper structure of the machine on the base carriage is provided by a hydraulic motor through a gear train. The other three links are operated through prismatic hydraulic actuators and as a result impose limits on the joint motion.

The whole machine can move forward or backward on its tracked undercarriage. This degree of freedom, will provide theoretically an infinite workspace for the machine. It can be easily seen that the structural and functional aspects of these machines are very similar to robots. Therefore, they are good candidates for applying the existing robotic technology. However, in the absence of the sensors to monitor and provide feedback of the environment in which they operate, these machines cannot be converted into fully automated robotic systems. In the following sections we will explain how the performance of these machines can be enhanced

[1] Spyder is manufactured by Kaiser Ltd.

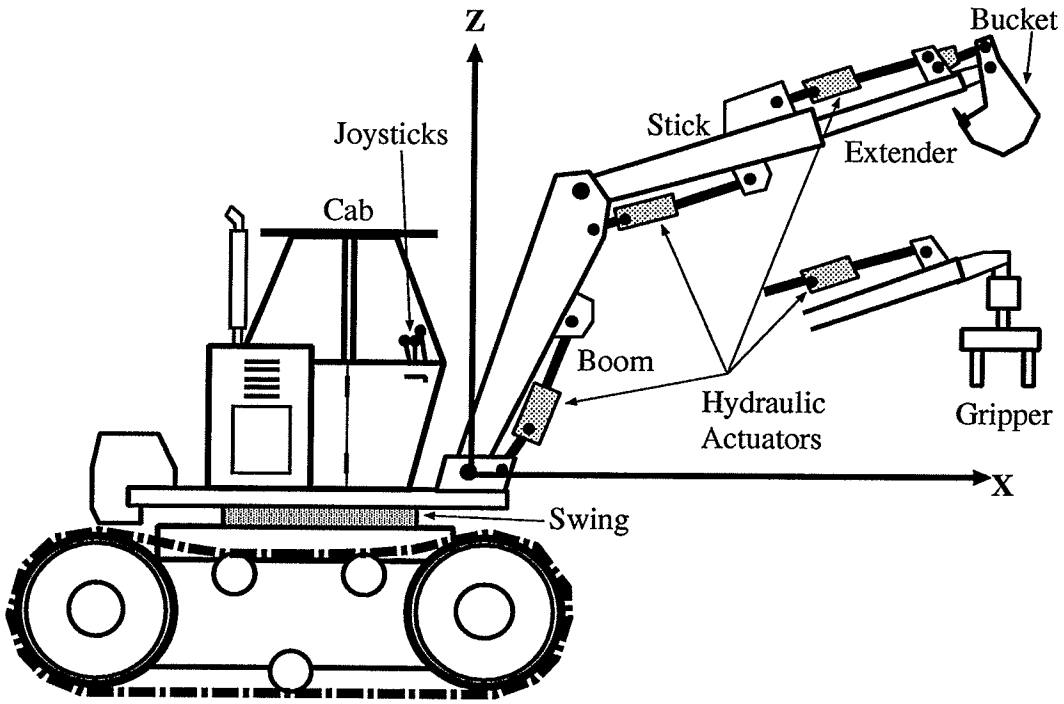

Figure 2.1: A typical heavy-duty industrial machine

by conversion of the basic motion from a "joint-mode" to a "coordinated-motion" control. These two types of motion are explained in the following sections.

2.1 Joint-mode Control

Joint-mode control is a one-to-one mapping between the control inputs and the link motions. For example each link of the machine shown in Figure 2.1 is controlled by a specific motion of the control lever that corresponds to that link. A displacement of the lever from its mid position produces a proportional velocity control command to each link.

Joint-mode control is easy to implement since it does not require any other control action to be generated. However, it requires the experience and skill of

the operator to produce proper coordination amongst the links. For example, to perform a task, such as scraping and leveling the ground, the operator brings the bucket closer to the base at a constant height, as well as maintaining a constant bucket angle with respect to the ground. The operator is required to simultaneously activate all the links by coordinating the motion of the control levers. The efficiency and accuracy of motion is thus directly dependent on the operator's skill. The control can be made much simpler by replacing joint-mode control with coordinated-motion control.

2.2 Coordinated-motion Control

The most natural way of operating the machine is to be able to move the joystick in a direction the end-effector is required to move. This could be achieved using a single joystick having three degree-of-freedom. The direction of the movement of the joystick indicates the direction in which the end-effector should move. This will reduce the level of coordination required to move the end-effector in any arbitrary direction. Under coordinated-motion control mode, the end-effector of the manipulator is controlled through velocity commands generated from the movement of the joystick.

In Coordinated-motion control the extent to which the joystick is moved from the mid position normally corresponds to the desired end-effector velocity in cartesian coordinate system ($\dot{X}, \dot{Y}$ and $\dot{Z}$). In situations when the operator is located within the cab and moves with the machine, the deflection of joystick is chosen to correspond to the end-effector movements in cylindrical coordinate

system ($\dot{R}, \dot{S}$ and $\dot{Z}$). In this case 'in/out' movement of the joystick gives the radial velocity, 'left/right' movement produces the proportional angular velocity and 'up/down' movement controls the velocity of the end-effector along vertical axis.

Figure 2.2 illustrates the various steps needed to control the end-effector of coordinated-motion controlled machine. The joystick is sampled to get the appropriate velocity commands in chosen coordinate system. Required joint angles and

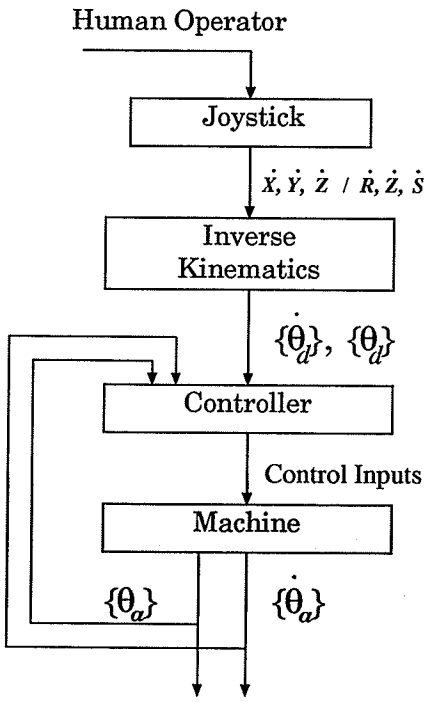

Figure 2.2: Steps involved in a coordinated-motion control.

joint velocities are then determined by solving the inverse kinematics of the machine. Finally, appropriate control inputs are calculated and sent to the machine. The second step in the sequence namely 'solving the inverse kinematics', is a key to many other issues dealt with in this thesis.

2.3 Redundancy in Manipulators

A manipulator which has more than the minimum number of joints required to track a desired trajectory, is called a redundant manipulator. Six degrees of freedom are needed for arbitrarily positioning and orienting an object. Therefore, a manipulator must have at least six joints to perform a task in three dimensional space to guarantee both position and orientation of the end-effector. In the case where the orientation is not critical, only three degrees of freedom are needed for positioning the object. Often manipulators are provided with more than the minimum number of joints required to perform a specific task . Additional joints, referred to as redundant joints, are normally utilized by the operator to avoid joint limits, obstacles and to improve the dexterity of the machine.

From a kinematic point of view the redundancy of a manipulator can result in an infinite number of possible joint velocities for a specified end-effector velocity. The right combination of joint velocities has to be determined through global or local optimization of a performance criterion (Kazerounian and Wang, 1987). Global optimization schemes (Nakamura *et al.*, 1987) are generally iterative and computationally complex. Hence they are limited to off-line control and programming only. Local optimization schemes, on the other hand, instantaneously determine a joint trajectory such that, at each point along the trajectory, a performance measure is locally optimized. The on-line implementation is essential if the end-effector position and trajectory are to be continuously modified based on feedback control system or by an operator. Several local optimization

schemes have been investigated which include weighted minimum-norm (Whitney, 1972), gradient projection scheme (Liegeois, 1977), extended Jacobian technique (Baillieul, 1985) and task priority-based redundancy control (Nakamura *et al.*, 1987).

The weighted minimum-norm solution minimizes the kinetic energy, with the inertia matrix as the weighted matrix. The gradient projection scheme optimizes a position-dependent scalar performance index by proper selection of a null space vector of the jacobian. The extended jacobian technique combines the kinematics and the optimization schemes into a set of equations whose unique solution maximizes a performance criterion. The task priority based concept, divides the task into subtasks according to the order of priority and determines the joint motions of robot manipulators based on the priority. Dubey *et al.* (1988) proposed an efficient implementation of the gradient projection scheme for manipulators with one degree of redundancy by introducing the concept of particular and homogeneous solutions that together optimize a scalar performance criterion. Zghal *et al.*, (1990) later extended this technique for multiple degrees of redundancy and utilized the gradient projection method to solve for the joint velocities subject to satisfying a performance criterion appropriate for joint limit avoidance.

Next Chapter will discuss the implementation of the gradient projection optimization technique to the class of machines under investigation.

CHAPTER 3

FORMULATION OF THE INVERSE KINEMATIC SOLUTION

This chapter describes the formulation of the inverse kinematic solution as applied to the class of heavy-duty redundant machines under investigation. A new performance criterion is presented to determine appropriate joint velocities and also to keep the various joints from reaching their limits. Previous investigations showed that hydraulic prismatic actuators used in heavy-duty hydraulic machines usually exhibit control problems near cylinder ends (Sepehri, 1990) and thus preventing them from reaching their limits is desirable from the control point of view.

The gradient projection technique is used to solve for the inverse kinematic solution while optimizing the new performance criterion. The method is basically a local optimization approach and therefore allows to achieve real-time computation. The real-time computation is essential since human is present in the control loop. The gradient optimization technique is described first in this chapter.

A new performance criterion that keeps the joints from reaching their limits as well produce smooth joint velocities by appropriate selection of the parameters introduced in the formulation will also be presented in this chapter. A novel algorithm is also developed, which in conjunction with the new criterion, will be able to utilize the overall hydraulic power more efficiently. This is followed by

demonstration of the scheme for efficient utilization of the coupled power. Finally, a scheme to have more control over individual joints, is included.

3.1 Gradient Projection Method

Consider an n degree-of-freedom manipulator having n joint coordinates θ_1 , θ_2 , $\cdots$, θ_n. The kinematic equation describing m independent variables denoting the end-effector displacement and orientation ($m \leq 6$), using these joints, ($n \geq m$) is given by

$$\dot{\mathbf{x}} = \mathbf{J}\,\dot{\Theta}\,, \tag{3.1}$$

where $\dot{\mathbf{x}}$ is an m-dimensional velocity vector consisting of translational and rotational velocities of the end-effector and $\dot{\Theta}$ is an n-dimensional joint velocity vector. The $(m \times n)$ matrix $\mathbf{J}$ is known as the Jacobian matrix.

If $\mathbf{J}$ is square (*i.e.*, $m = n$) and of full rank, it could be inverted to evaluate the unique set of joint velocities $\dot{\Theta}$, required to achieve the desired end-effector motion $\dot{\mathbf{x}}$ (Inverse kinematic solution). On the other hand, if $\mathbf{J}$ is singular or rectangular (*i.e.*, $m < n$), there exist an infinite joint velocity solutions $\dot{\Theta}$, that satisfy Equation (3.1). For such cases Whitney (1969) has shown that a solution that minimizes the norm of the joint velocity vector ($\dot{\Theta}^T\dot{\Theta}$) is determined by

$$\dot{\Theta}_{MN} = \mathbf{J}^{+}\dot{\mathbf{x}}\,, \tag{3.2}$$

$$\mathbf{J}^{+} = \mathbf{J}^{T}\left(\mathbf{J}\,\mathbf{J}^{T}\right)^{-1}. \tag{3.3}$$

$\mathbf{J}^{+}$ is the Moore-Penrose generalized inverse or pseudoinverse of the Jacobian $\mathbf{J}$.

A more general solution was later proposed which determines $\dot{\Theta}$ by minimizing or maximizing a given objective function $H = H(\Theta)$. The objective function is formulated based on some criteria to improve the performance of the manipulator; e.g., preventing joint limits, avoiding singularity, etc. The solution namely, 'gradient projection method' (Ben-Israel and Greville 1974 and Liegeois 1977) is formulated as below:

$$\dot{\Theta} = \mathbf{J}^{+}\dot{\mathbf{x}} + k(\mathbf{I} - \mathbf{J}^{+}\mathbf{J})\,\nabla H\,, \tag{3.4}$$

where $\mathbf{I}$ is an $(n \times n)$ identity matrix, $(\mathbf{I} - \mathbf{J}^{+}\mathbf{J})$ is the null space projection matrix and ∇H is the gradient vector of H given as:

$$\nabla H = \left[\frac{\partial H}{\partial \theta_1} \;\; \frac{\partial H}{\partial \theta_2} \;\; \cdots \;\; \frac{\partial H}{\partial \theta_i} \;\; \cdots \;\; \frac{\partial H}{\partial \theta_n}\right]^{T}. \tag{3.5}$$

The scalar k in Equation (3.4) is a gain constant. k is positive when H is to be maximized and negative, otherwise. A larger value of k will optimize H at a faster rate. However, k is limited by bounds on the joint velocities (Euler *et al.*, 1988).

Referring to Equation (3.4), the solution obtained by gradient projection method consists of two terms. The first term, $\mathbf{J}^{+}\dot{\mathbf{x}}$, is the minimum-norm least-squares solution shown in Equation (3.4). The second term, $(\mathbf{I} - \mathbf{J}^{+}\mathbf{J})\,\nabla H$, is a homogeneous solution in the null space of Jacobian $\mathbf{J}$, which corresponds to the manipulator's self motion. Self motion is a set of joint motions that does not contribute to the end-effector motion.

The initial attempt to apply Equation (3.4) was computationally complex and did not allow for real-time implementation (Klein and Huang, 1983). An efficient

implementation of this scheme for one degree of redundancy was first proposed by Dubey *et al.*, (1988). The approach was later extended for manipulators having multiple degrees of redundancy (Zghal *et al.*, 1990). One advantage of this implementation is that it does not require the computation of the pseudoinverse Jacobian $\mathbf{J}^+$, and thus allows more efficient formulation for determining the joint velocities. This scheme is detailed in the following section.

3.2 Efficient Solution to Gradient Projection Method

The approach is based on the fact that a joint velocity vector $\dot{\Theta}$ satisfying Equation (3.1) can be expressed as

$$\dot{\Theta} = \dot{\Theta}_{\mathbf{p}} + \dot{\Theta}_{\mathbf{h}}\,, \tag{3.6}$$

where $\dot{\Theta}_{\mathbf{p}} \in R^n$ is a particular solution of Equation (3.1) and $\dot{\Theta}_{\mathbf{h}} \in R^n$ is a homogeneous solution satisfying

$$\mathbf{J}\,\dot{\Theta}_{\mathbf{h}} = \mathbf{O}^{(m\times 1)}\,, \tag{3.7}$$

with $\mathbf{O} \in R^m$ being the zero vector.

In order to solve for $\dot{\Theta}_{\mathbf{p}}$ and $\dot{\Theta}_{\mathbf{h}}$, the Jacobian $\mathbf{J}$ is partitioned into a non-singular square matrix $\mathbf{J}_1$ and the remaining matrix $\mathbf{J_0}$. $\mathbf{J}_1$ contains any m independent columns of the Jacobian $\mathbf{J}$. The remaining r columns of $\mathbf{J}$ are expressed as an $(m \times r)$ matrix $\mathbf{J}_0$. Here $r = n - m$ is the number of degrees of redundancy. By rearranging the columns of $\mathbf{J}$ and the corresponding elements of $\dot{\Theta}$, Equation

(3.1) can be rewritten as:

$$\dot{\mathbf{x}} = \begin{bmatrix} \mathbf{J}_0^{(m\times r)} & \mathbf{J}_1^{(m\times m)} \end{bmatrix} \dot{\Theta}\,. \tag{3.8}$$

It is noted that a singularity analysis is required to determine the conditions under which m independent column vectors can always be found. Different column arrangements, each corresponding to a different singularity condition of $\mathbf{J}_1$, may be considered to constantly produce a non-singular square matrix $\mathbf{J}_1$.

The particular solution $\dot{\Theta}_\mathbf{p}$ is obtained by setting the first r elements of $\dot{\Theta}_\mathbf{p}$ to zeros, and solving Equation (3.8) for the remaining m elements. The solution is represented as follows:

$$\dot{\Theta}_\mathbf{p} = \begin{bmatrix} \mathbf{O}^{(r\times 1)} \\ \left[\mathbf{J}_1^{(m\times m)}\right]^{-1}\ \dot{\mathbf{x}}^{(m\times 1)} \end{bmatrix}. \tag{3.9}$$

The homogeneous solution $\dot{\Theta}_\mathbf{h}$ is an element of the r-dimensional null space of $\mathbf{J}$. Assuming that the null space of $\mathbf{J}$ is spanned by a linearly independent set of r joint velocity vectors, namely $\dot{\Theta}_{\mathbf{h}1},\ \dot{\Theta}_{\mathbf{h}2},\ \cdots,\ \dot{\Theta}_{\mathbf{h}r}$, the homogeneous solution $\dot{\Theta}_\mathbf{h}$ is given by

$$\begin{aligned} \dot{\Theta}_\mathbf{h} &= \kappa_1\,\dot{\Theta}_{\mathbf{h}1} + \kappa_2\,\dot{\Theta}_{\mathbf{h}2} + \cdots + \kappa_r\,\dot{\Theta}_{\mathbf{h}r} = \sum_{s=1}^{r} \kappa_s\,\dot{\Theta}_{\mathbf{h}s}\,, \\ &= \begin{bmatrix} \dot{\Theta}_{\mathbf{h}1}\ \dot{\Theta}_{\mathbf{h}2}\ \cdots\ \dot{\Theta}_{\mathbf{h}r} \end{bmatrix} \vec{\kappa}\,, \end{aligned} \tag{3.10}$$

where $\vec{\kappa} = [\kappa_1\ \kappa_2\ \cdots\ \kappa_r]^T$ is a real vector. The homogeneous solution $\dot{\Theta}_{\mathbf{h}}$ can be determined by assuming the first r elements of $\dot{\Theta}_{\mathbf{h}}$ to be equal to the respective elements of vector $\vec{\kappa}$, and solving Equation (3.7) for the remaining $(n-r)$ elements results in:

$$\dot{\Theta}_{\mathbf{h}} = \begin{bmatrix} \mathbf{I}^{(r\times r)} \\ \\ -\left[\mathbf{J}_1^{(m\times m)}\right]^{-1}\ \mathbf{J}_0^{(m\times r)} \end{bmatrix} \vec{\kappa}^{(r\times 1)}. \tag{3.11}$$

Note that the column vectors of the $(n \times r)$ matrix shown in the bracket on the right-hand-side of Equation (3.11) make up the set of linearly independent homogeneous solutions $(\dot{\Theta}_{\mathbf{h}1},\ \dot{\Theta}_{\mathbf{h}2},\ \cdots, \dot{\Theta}_{\mathbf{h}r})$. This then sets the basis for the null space of $\mathbf{J}$. Substituting Equation (3.9) and (3.11) into Equation (3.6) yields the following joint velocity solution:

$$\dot{\Theta} = \dot{\Theta}_{\mathbf{p}} + \sum_{s=1}^{r} \kappa_s\, \dot{\Theta}_{\mathbf{h}s} = \begin{bmatrix} \vec{\kappa} \\ \\ [\mathbf{J}_1]^{-1}\ (\dot{\mathbf{x}} - \mathbf{J}_0\, \vec{\kappa}) \end{bmatrix}. \tag{3.12}$$

In order to find the minimum-norm least squares solution for joint velocity vector as in Equation (3.3), the values of κ_s $(s = 1, 2, \cdots, r)$ are calculated to minimize the square of the norm of $\dot{\Theta}$. This is achieved by taking the partial derivatives of the right side of Equation (3.12) with respect to κ_s and equating

them to zero as shown below;

$$\frac{\partial\|\dot{\Theta}\|^2}{\partial \kappa_s} = \frac{\partial\left(\dot{\Theta}^T\dot{\Theta}\right)}{\partial \kappa_s} = 2\left(\dot{\Theta}_{\mathbf{p}} + \sum_{i=1}^{r} \kappa_i \dot{\Theta}_{\mathbf{h}i}\right)^T \dot{\Theta}_{\mathbf{h}s} = 0\,, \quad s = 1, 2, \ldots r. \tag{3.13}$$

If the set of homogeneous solutions ($\dot{\Theta}_{\mathbf{h}1}$, $\dot{\Theta}_{\mathbf{h}2}$, $\cdots$, $\dot{\Theta}_{\mathbf{h}r}$) is orthogonal to the Jacobian, the scalar constants κ_s can be solved as (Zghal *et al.*, 1990);

$$\kappa_s = -\frac{\dot{\Theta}_{\mathbf{p}}{}^T\,\dot{\Theta}_{\mathbf{h}s}}{\dot{\Theta}_{\mathbf{h}s}{}^T\,\dot{\Theta}_{\mathbf{h}s}}\,. \tag{3.14}$$

Hence, the minimum-norm least-squares joint velocity vector solution, $\dot{\Theta}_{MN}$, expressed in terms of the particular solution, $\dot{\Theta}_{\mathbf{p}}$, and the orthogonal set of homogeneous solutions, $\dot{\Theta}_{\mathbf{h}1}$, $\dot{\Theta}_{\mathbf{h}2}$, $\cdots$, $\dot{\Theta}_{\mathbf{h}r}$, is given by;

$$\begin{aligned}\dot{\Theta}_{MN} &= \dot{\Theta}_{\mathbf{p}} - \left[\sum_{s=1}^{r} \frac{\dot{\Theta}_{\mathbf{p}}{}^T\,\dot{\Theta}_{\mathbf{h}s}}{\dot{\Theta}_{\mathbf{h}s}{}^T\,\dot{\Theta}_{\mathbf{h}s}}\dot{\Theta}_{\mathbf{h}s}\right], \\ &= \dot{\Theta}_{\mathbf{p}} - \sum_{s=1}^{r}\left(\dot{\Theta}_{\mathbf{p}}{}^T\,\hat{\mathbf{u}}_s\right)\hat{\mathbf{u}}_s\,,\end{aligned} \tag{3.15}$$

where $\hat{\mathbf{u}}_s$ is the unit vector in the direction of $\dot{\Theta}_{\mathbf{h}s}$, and is given by:

$$\hat{\mathbf{u}}_s = \frac{\dot{\Theta}_{\mathbf{h}s}}{\sqrt{\dot{\Theta}_{\mathbf{h}s}{}^T\,\dot{\Theta}_{\mathbf{h}s}}}\,. \tag{3.16}$$

Referring to Equation (3.15), the minimum-norm least-squares solution is obtained by subtracting from the particular solution of $\dot{\Theta}_{\mathbf{p}}$, its components along the orthogonal homogeneous solutions. It is clear that the orthogonality of the homogeneous solution is necessary, so that subtracting from $\dot{\Theta}_{\mathbf{p}}$ its component along one homogeneous solution, will not produce any new components in other directions of the homogeneous solutions.

The next step is to find the joint velocity solution given by Equation (3.4)

for optimizing the performance criterion $H(\Theta)$. To obtain this, the projection of the gradient vector ∇H onto the null space of $\mathbf{J}$, is added to the minimum-norm solution given by Equation (3.6). The solution to the projection of the gradient vector ∇H onto the null space of $\mathbf{J}$ can be shown to be as follows (Zghal*et. al.*, 1990):

$$\begin{aligned}(\mathbf{I}-\mathbf{J}^{+}\mathbf{J})\nabla H &= \sum_{s=1}^{r}\left(\frac{\nabla H^{T}\,\dot{\Theta}_{\mathbf{h}s}}{\dot{\Theta}_{\mathbf{h}s}{}^{T}\,\dot{\Theta}_{\mathbf{h}s}}\right)\dot{\Theta}_{\mathbf{h}s}\,,\\ &= \sum_{s=1}^{r}\left(\nabla H^{T}\,\hat{\mathbf{u}}_{s}\right)\hat{\mathbf{u}}_{s}\,. \qquad (3.17)\end{aligned}$$

Adding the solution represented by Equation (3.17) to the minimum-norm solution given in Equation (3.15) results in

$$\begin{aligned}\dot{\Theta} &= \dot{\Theta}_{\mathbf{p}}-\sum_{s=1}^{r}\left(\dot{\Theta}_{\mathbf{p}}{}^{T}\,\hat{\mathbf{u}}_{s}\right)\hat{\mathbf{u}}_{s}+k\sum_{s=1}^{r}\left(\nabla H^{T}\,\hat{\mathbf{u}}_{s}\right)\hat{\mathbf{u}}_{s}\\ &= \dot{\Theta}_{\mathbf{p}}-\sum_{s=1}^{r}\left[\left(\dot{\Theta}_{\mathbf{p}}{}^{T}\,\hat{\mathbf{u}}_{s}\right)+k\left(\nabla H^{T}\,\hat{\mathbf{u}}_{s}\right)\right]\,\hat{\mathbf{u}}_{s}\,. \qquad (3.18)\end{aligned}$$

The value of k may be determined based on joint velocity bounds (see Euler *et al.*, 1988).

3.3 Joint Limit Avoidance Criteria (H)

3.3.1 Previous Work

The performance of the redundant manipulator may be judged in terms of a performance criterion such as avoiding the joint limits. Liegeois (1977) proposed the following performance criterion which takes into account the joint's distance from their limits.

$$H_1(\theta_j) = \frac{1}{n}\sum_{j=1}^{n}\left(\frac{\theta_{j,Max} - 2\theta_j + \theta_{j,Min}}{\theta_{j,Max} - \theta_{j,Min}}\right)^2, \tag{3.19}$$

where n is the number of joints ($n = 4$ for Kaiser Spyder), θ_j is the current joint angle and, θ_{jMax} and θ_{jMin} are the upper and the lower limits on θ_j, respectively. Minimizing the above criterion will prevent the joints from reaching their physical bounds. The gradient of H_1 is a vector given by:

$$\nabla H_1 = \left[\frac{\partial H_1}{\partial \theta_1} \quad \frac{\partial H_1}{\partial \theta_2} \quad \cdots \quad \frac{\partial H_1}{\partial \theta_n}\right]^T \tag{3.20}$$

where

$$\frac{\partial H_1}{\partial \theta_j} = \left(\frac{1}{n}\right)\frac{-4(\theta_{j,Max} - 2\theta_j + \theta_{j,Min})}{(\theta_{j,Max} - \theta_{j,Min})^2}, \quad j = 1, 2, \ldots, n. \tag{3.21}$$

This criterion and its gradient for various joint positions, is graphically shown in Figure 3.1. As shown in the figure, the gradient of the criterion assigns to each joint, a weight which is linearly proportional to the distance of the joint from its mid-range value.

Klein and Chirco (1987) suggested the following measure of joint range avail-

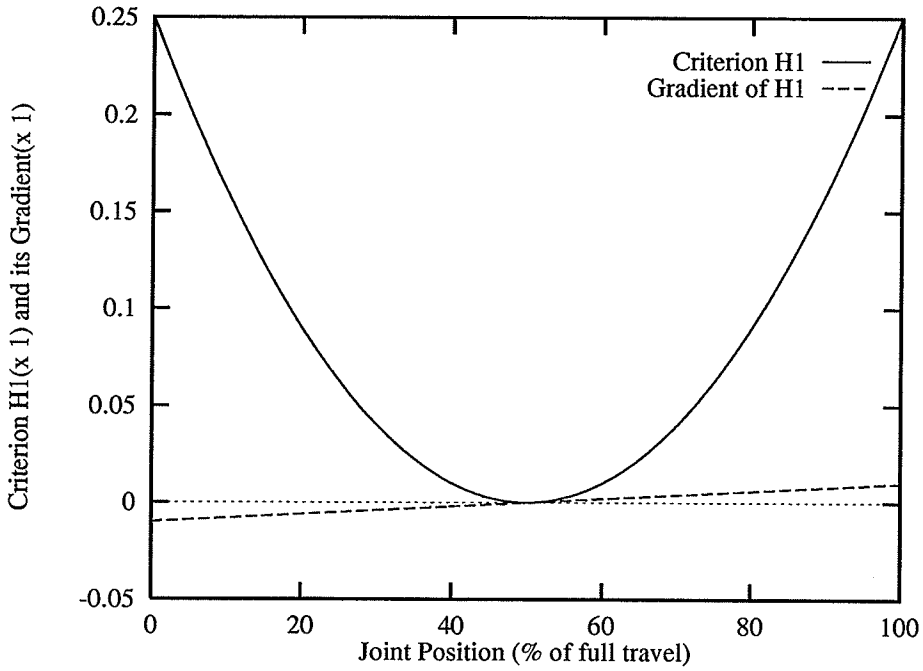

Figure 3.1: Criterion H_1 and its Gradient

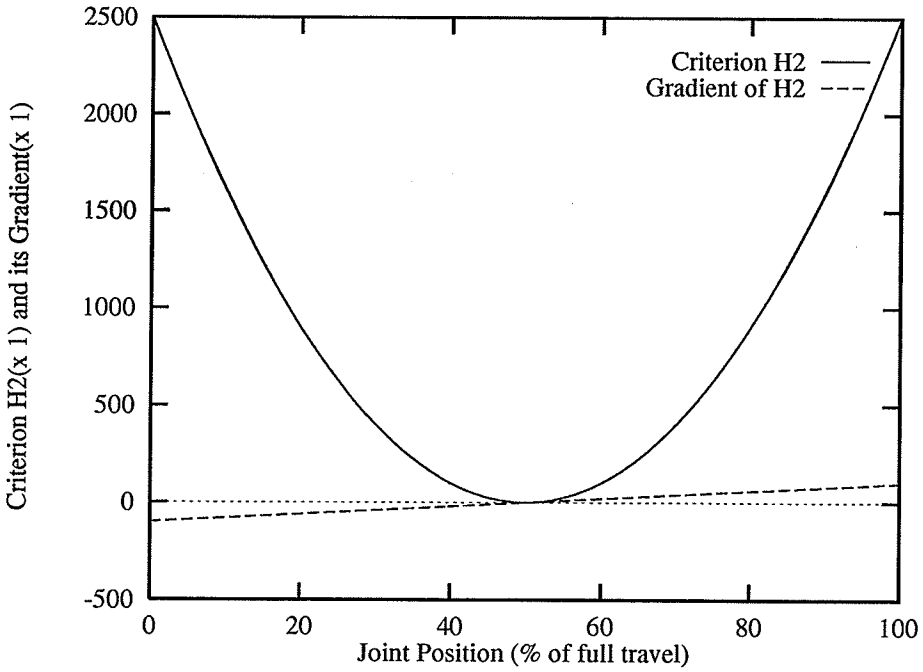

Figure 3.2: Criterion H_2 and its Gradient

ability:

$$H_2(\theta_j) = \sum_{j=1}^{n} (\theta_j - \theta_{j,c})^2 \,. \tag{3.22}$$

where $\theta_{j,c}$ is the desired joint angle state and is normally chosen as the middle of the joint range. The gradient of H_2 is

$$\frac{\partial H_2}{\partial \theta_j} = 2(\theta_j - \theta_{j,c}), \qquad j = 1, 2, \ldots, n. \tag{3.23}$$

The characteristic of H_2, described by Equation (3.22), is graphically shown in Figure 3.2. It is seen that this formulation also assigns to each joint a weight proportional to the joint distance from the desired joint state.

Referring to Figures 3.1 and 3.2, both criteria H_1 and H_2 appear to be identical. However, since $H_2 >> H_1$, the performance criterion H_2 will result in optimizing the joint limits faster if k in Equation (3.18) is not calculated based on joint velocity bounds. When k is determined based on maximum joint velocity limits (for example using method proposed by Euler *et. al.*, 1988), H_1 and H_2 will be scaled proportionally and will produce similar results.

A third performance criterion was later introduced by Zghal *et al.*, (1990):

$$H_3(\theta_j) = \sum_{j=1}^{n} \frac{(\theta_{j,Max} - \theta_{j,Min})^2}{(\theta_{j,Max} - \theta_j)(\theta_j - \theta_{j,Min})} \,. \tag{3.24}$$

The gradient of H_3 is given as:

$$\frac{\partial H_3}{\partial \theta_j} = \frac{(\theta_{j,Max} - \theta_{j,Min})^2(\theta_{j,Max} - 2\theta_j + \theta_{j,Min})}{[(\theta_{j,Max} - \theta_j)(\theta_j - \theta_{j,Min})]^2}, \quad j = 1, 2, \ldots, n \,. \tag{3.25}$$

This criterion is shown in Figure 3.3. The gradient is not linear and assigns higher

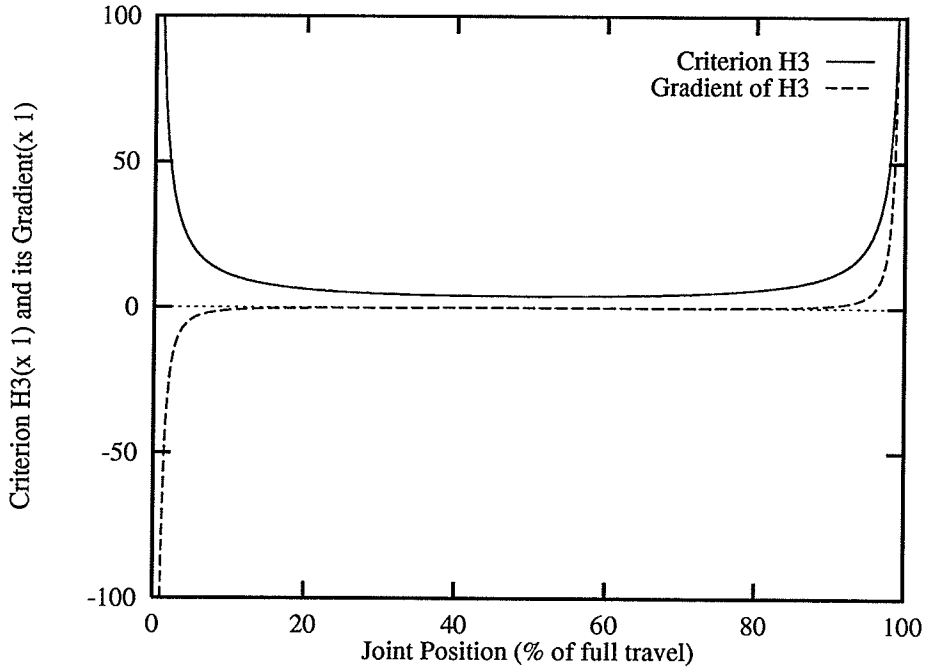

Figure 3.3: Criterion H_3 and its Gradient

values when the joint approaches the joint limits.

3.3.2 New Performance Criterion

During the course of this study, a more general performance criterion namely $H_4(\theta_j)$ was developed which was found to be most appropriate for the purpose of our application:

$$H_4(\theta_j) = \sum_{j=1}^{n} \cosh\left(\phi \frac{\theta_j - \theta_{j,c}}{\theta_{j,Max} - \theta_{j,Min}}\right), \tag{3.26}$$

where $\theta_{j,c}$ is the desired joint angle state and is normally chosen as the middle of the joint range. The new performance criterion is a hyperbolic function of the

joint angles and is to be minimized. The gradient of H_4 is:

$$\frac{\partial H_4}{\partial \theta_j} = \frac{\phi}{\theta_{j,max} - \theta_{j,min}} \sinh\left(\phi \frac{\theta_j - \theta_{j,c}}{\theta_{j,max} - \theta_{j,min}}\right). \tag{3.27}$$

Referring to Equation 3.26 a factor ϕ is introduced which allows better control over the joint limit avoidance capacity of the criterion. Figures 3.4, 3.5, 3.6 and 3.7 shows how ϕ affects the performance of H_4. As seen from Figure 3.4, at lower values of ϕ, criterion H_4 is nearly linear and performs similar to criteria H_1 and H_2. As ϕ increases (see Figures 3.5 to 3.7), the criterion assigns higher and higher values to joints as they approach their limits. As a result the joint limit avoidance capability of the criterion increases with ϕ. However, as will be demonstrated later, a lower value of ϕ generates gradually changing joint velocities but may not effectively avoid the joints from reaching their limits. The joint limit capability can be enhanced using higher values of ϕ, at the cost of gradually changing joint velocities.

The new gradient of new criterion is compared to other criterion in Figure 3.3.2. As is clear from the fugure the criterion can be configured to set the joint limit avoidance capability by selecting a suitable value of ϕ. The performance of all the criteria discussed in this section will be evaluated with an example in Section 4.3.

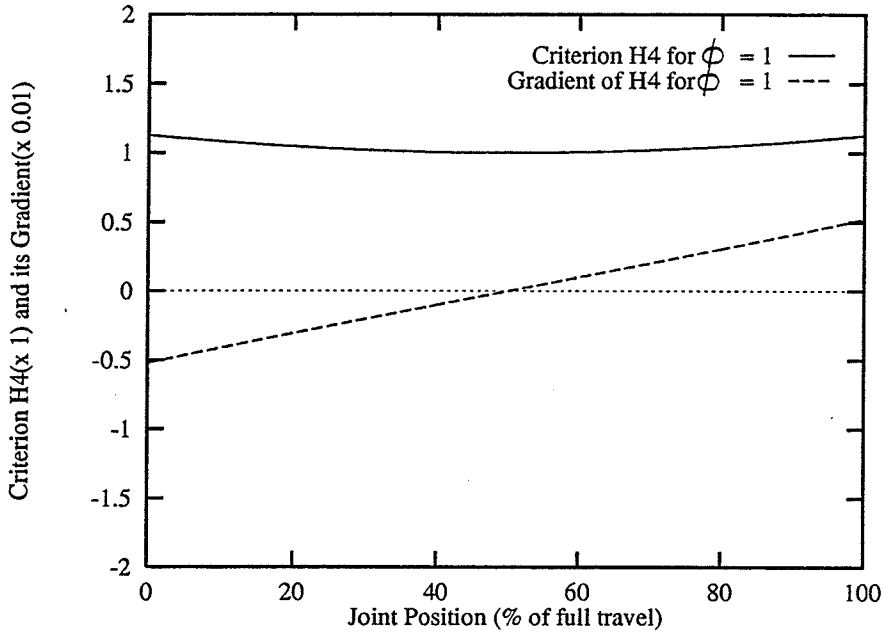

Figure 3.4: Criterion H_4 and its Gradient for $\phi = 1$

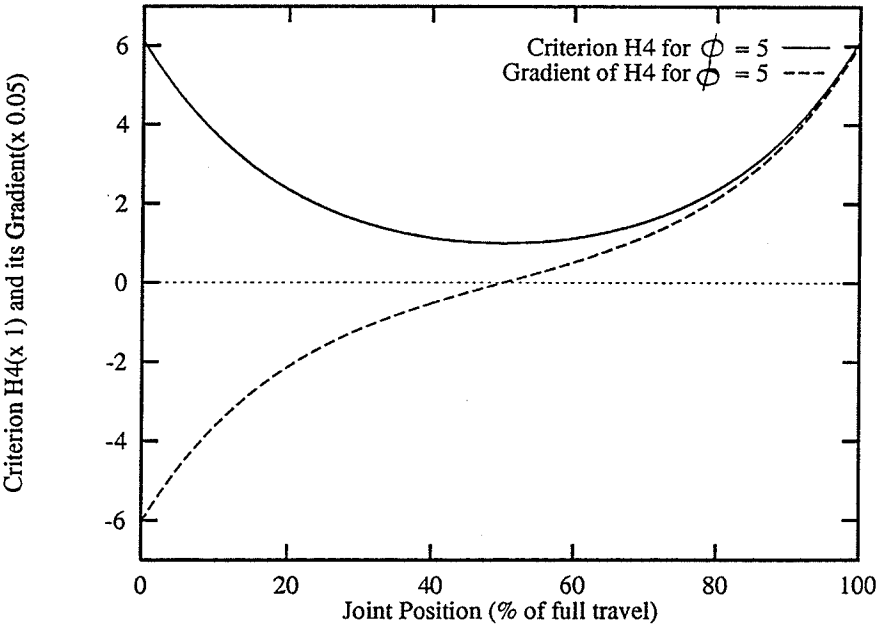

Figure 3.5: Criterion H_4 and its Gradient for $\phi = 5$

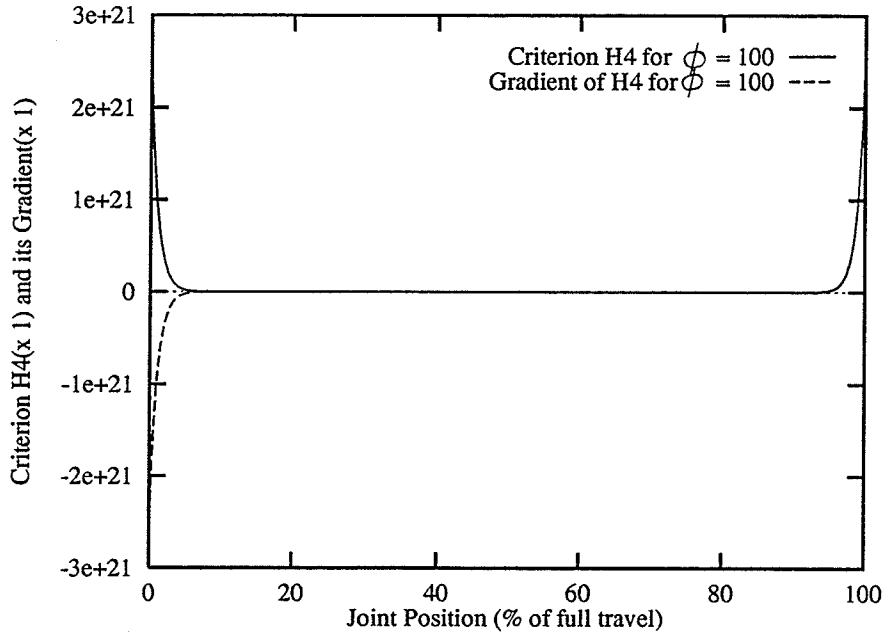

Figure 3.6: Criterion H_4 and its Gradient for $\phi = 15$

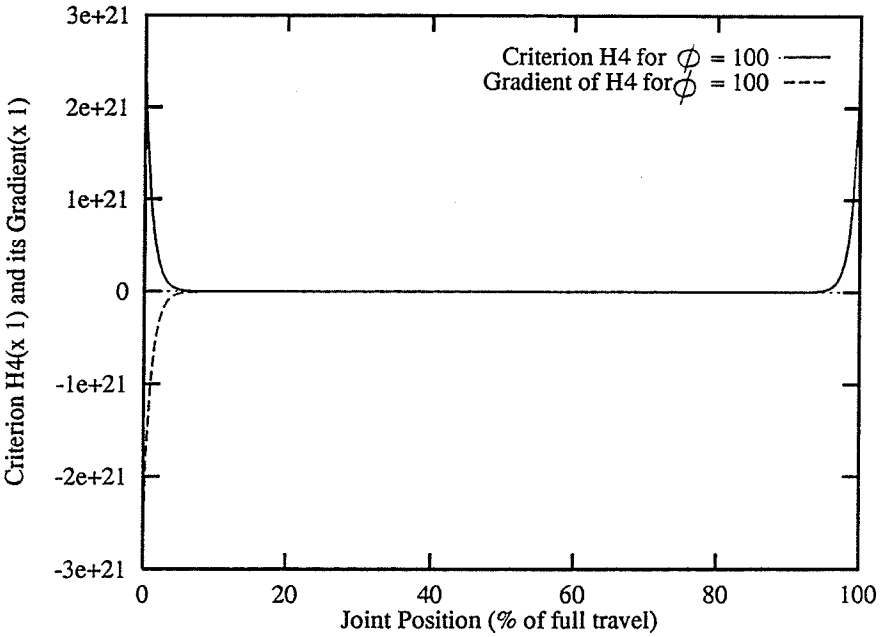

Figure 3.7: Criterion H_4 and its Gradient for $\phi = 100$

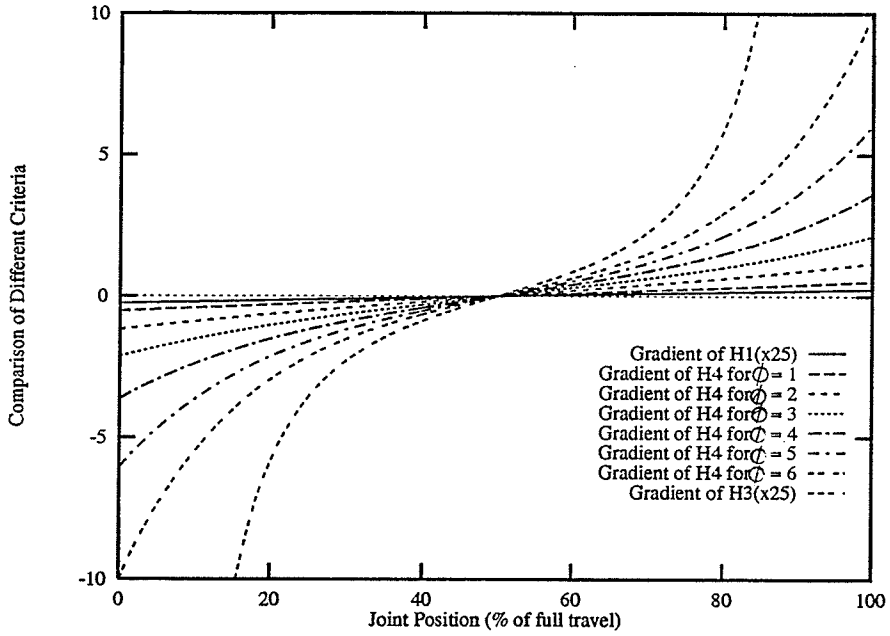

Figure 3.8: Comparison of Different performance criteria

3.4 Implementation to Industrial Machines

In this section, the gradient optimization technique is applied to solve the inverse kinematics of a Kaiser Spyder machine shown in Figure 2.1. The focus will be on the application of the proposed performance criterion, formulated in Equation (3.26). The scheme is implemented both in Cartesian and Cylindrical coordinate systems. For the case when operator is not present on the machine, his/her commands will be interpreted in Cartesian coordinates; i.e., the 'up/down' movement of the joystick represents the motion of the end-effector along the **Z** axis (see Figure 2.1) while the 'left/right' and 'in/out' motions of joystick will produce the motion along the **X** and **Y** axis, respectively.

For the case when operator is present on the machine, the joystick commands will be interpreted in Cylindrical coordinates; i.e., the 'left/right' motion of the joystick will produce the rotation of the machine about a vertical axis, the 'up/down' motion of the joystick will control the height of the end-effector and the 'in/out' motion of joystick will control the radial motion of the end-effector. The kinematic parameters of the Spyder are shown in Appendix A.

3.4.1 Cartesian Coordinate Mode

Controlling the three Cartesian variables corresponding to the translational motion of the end-effector of a stationary Spyder machine, results in one degree of redundancy. This redundant joint can be used to improve the manipulator's performance by avoiding the joints from reaching their limits. In such a case the

kinematic solution given by Equation (3.1) reduces to

$$\mathbf{v_T} = \mathbf{J}_T \, \dot{\Theta}_T \,, \tag{3.28}$$

where $\mathbf{v_T} = [\dot{\mathbf{X}}, \dot{\mathbf{Y}}, \dot{\mathbf{Z}}]^{\mathbf{T}}$ is the translational velocity vector in Cartesian workspace of the Spyder's end-effector and $\mathbf{J}_T$ is the (3×4) Jacobian associated with the translational motion of the end-effector. The derivation of $\mathbf{J}_T$ is given in Appendix A. $\mathbf{J}_T$ can also be written as

$$\mathbf{J}_T = \begin{bmatrix} \mathbf{J}_{T1} & \mathbf{J}_{T2} & \mathbf{J}_{T3} & \mathbf{J}_{T4} \end{bmatrix} \tag{3.29}$$

where $\mathbf{J}_{Ti}$ represents the contribution of the i^{th} joint to the end-effector's translational motion. The joint velocity vector $\dot{\Theta}_T \in R^4$ contains the three revolute joint velocities $\dot{\theta}_1, \dot{\theta}_2, \dot{\theta}_3$ and a prismatic joint velocity $\dot{d}_4$. From Equation 3.4, the joint velocity vector $\dot{\Theta}_T$ for optimizing a performance criterion $H(\Theta_T)$ is

$$\dot{\Theta}_T \;=\; \mathbf{J}_T^{+} \, \mathbf{v_T} \;+\; k(\mathbf{I} - \mathbf{J}_T^{+} \, \mathbf{J}_T) \, \nabla H \,. \tag{3.30}$$

The non-singular (3×3) matrix $\mathbf{J}_1$ is constructed from any three independent columns of $\mathbf{J}_T$, and the remaining column makes up the vector $\mathbf{J}_0$. Thus, Equation (3.28) can be rewritten as:

$$\mathbf{v_T} = \begin{bmatrix} \mathbf{J}_0^{3\times 1} & \mathbf{J}_1^{3\times 3} \end{bmatrix} \, \dot{\Theta}_T \,. \tag{3.31}$$

Note that the elements of $\dot{\Theta}_T$ are rearranged to be of the same order as the columns of the matrix on the right side of (3.31). For the Spyder, four arrangements of the columns of $\mathbf{J}_T$ are possible. Simulation studies have shown that the following arrangement

$$\mathbf{J}_0 = \mathbf{J}_{T1} \quad \text{and} \quad \mathbf{J}_1 = \begin{bmatrix} \mathbf{J}_{T2} & \mathbf{J}_{T3} & \mathbf{J}_{T4} \end{bmatrix}, \tag{3.32}$$

results in a singular matrix $\mathbf{J}_1$. The other three arrangements result in different algorithmic singularities; however, switching amongst them will avoid possible singularities.

Using the solution obtained in (3.18), the joint velocity vector $\dot{\Theta}_T$ can be found to be:

$$\dot{\Theta}_T = \dot{\Theta}_{\mathbf{p},T} - \left[\left(\dot{\Theta}_{\mathbf{p},T}{}^T \, \hat{\mathbf{u}}_T \right) + k \left(\nabla H^T \, \hat{\mathbf{u}}_T \right) \right] \hat{\mathbf{u}}_T \,, \tag{3.33}$$

where $\dot{\Theta}_{\mathbf{p},T}$ is the particular solution given by

$$\dot{\Theta}_{\mathbf{p},T} = \begin{bmatrix} \mathbf{O}^{(1\times 1)} \\ \\ \left[\mathbf{J}_1^{(3\times 3)}\right]^{-1} \, \mathbf{V_T}^{(3\times 1)} \end{bmatrix}. \tag{3.34}$$

$\hat{\mathbf{u}}_T$ is the unit vector in the direction of the homogeneous solution $\dot{\Theta}_{\mathbf{h},T}$ (see

Equation 3.15), and is given by

$$\dot{\Theta}_{\mathbf{h},T} = \begin{bmatrix} \mathbf{I}^{(1\times1)} \\ -\left[\mathbf{J}_1^{(3\times3)}\right]^{-1} \mathbf{J}_0^{(3\times1)} \end{bmatrix}. \tag{3.35}$$

3.4.2 Cylindrical Coordinate Mode

In the case when operator is present in the machine, the algorithm utilizes cylindrical coordinates. Note that in Cartesian coordinates the size of the Jacobian matrix $\mathbf{J}$ was (3×4). In Cylindrical coordinates the Jacobian is reduced to a (2×3) matrix. This is due to the fact that the workspace in Cylindrical coordinates can be represented by a vertical plane and rotation of this plane about a vertical axis (see Figure 3.9). Since the 'left/right' motion of the joystick is directly assigned to the rotation of the cabin, only two variables S and S are left to be controlled in a vertical plane using three links (boom, stick and extender). In this case the 'left/right, motion of the joystick corresponds to the peripheral velocity $\dot{S} = R\dot{\theta}_1$ and not the angular velocity $\dot{\theta}_1$ of the swing. The angular velocity $\dot{\theta}_1$ is equal to $\dot{S}/R$, where R is the radial distance of the end-effector from the axis of rotation (see Figure 3.9). The kinematic equation given by (3.1), then reduces to

$$\mathbf{v_R} = \mathbf{J}_R\, \dot{\Theta}_R\,, \tag{3.36}$$

where $\mathbf{v_R}$ is the translational velocity in a vertical plane and $\mathbf{J}_R$ is the (2×3) Jacobian associated with the translational motion of the end-effector in a vertical plane. The derivation of $\mathbf{J}_R$ is given in Appendix A. The Jacobian $\mathbf{J}_R$ can also be

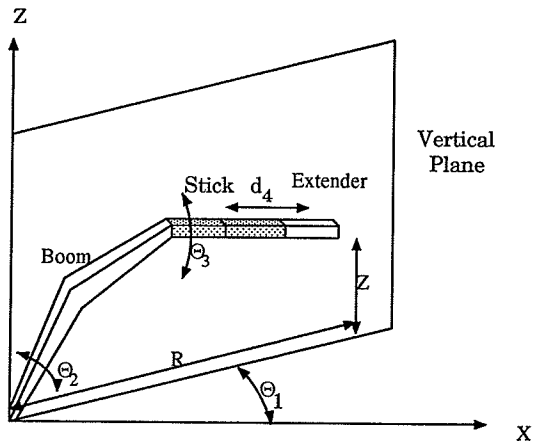

Figure 3.9: Manipulator in Cylindrical coordinates

written as:

$$\mathbf{J}_R = \begin{bmatrix} \mathbf{J}_{R2} & \mathbf{J}_{R3} & \mathbf{J}_{R4} \end{bmatrix} , \tag{3.37}$$

where $\mathbf{J}_{Ri}$ represents the contribution of the i^{th} joint to the end-effector motion in the vertical plane. The joint velocity vector $\dot{\Theta}_R \in R^3$ contains the two revolute joint velocities $\dot{\theta}_2, \dot{\theta}_3$ and a prismatic joint velocity $\dot{d}_4$. The joint velocity vector $\dot{\Theta}_R$ for optimizing a performance criterion $H(\Theta_R)$ is given by

$$\dot{\Theta}_R \;=\; \mathbf{J}_R^{+}\, \mathbf{v_R} \;+\; k(\mathbf{I} - \mathbf{J}_R^{+}\, \mathbf{J}_R)\, \nabla H\,. \tag{3.38}$$

The non-singular (2×2) matrix $\mathbf{J}_1$ is constructed from any two independent columns of $\mathbf{J}_R$ and the remaining column form $\mathbf{J}_0$. Equation (3.36) can then be

written as:

$$\mathbf{v_R} = \begin{bmatrix} \mathbf{J}_0^{2\times 1} & \mathbf{J}_1^{2\times 2} \end{bmatrix} \dot{\Theta}_R . \tag{3.39}$$

The elements of $\dot{\Theta}_R$ are rearranged to be of the same order as the columns of the matrix on the right side of (3.39). For the Spyder machine, three arrangements of the columns of $\mathbf{J}_R$ are possible. The preliminary studies have shown that the first arrangement

$$\mathbf{J}_0 = \mathbf{J}_{R2} \quad \text{and} \quad \mathbf{J}_1 = \begin{bmatrix} \mathbf{J}_{R3} & \mathbf{J}_{R4} \end{bmatrix} , \tag{3.40}$$

results in a non-singular matrix $\mathbf{J}_1$, most of the times. The other two arrangements result in different algorithmic singularities and switching amongst them will avoid all these singularities. Using the solution obtained in (3.18), the joint velocity vector $\dot{\Theta}_R$ is found to be

$$\dot{\Theta}_R = \dot{\Theta}_{\mathbf{p},R} - \left[\left(\dot{\Theta}_{\mathbf{p},R}{}^T \, \hat{\mathbf{u}}_R \right) + k \left(\nabla H^T \, \hat{\mathbf{u}}_R \right) \right] \hat{\mathbf{u}}_R . \tag{3.41}$$

where $\dot{\Theta}_{\mathbf{p},R}$ is the particular solution

$$\dot{\Theta}_{\mathbf{p},R} = \begin{bmatrix} \mathbf{O}^{(1\times 1)} \\ \left[\mathbf{J}_1^{(2\times 2)} \right]^{-1} \mathbf{v_R}^{(2\times 1)} \end{bmatrix} , \tag{3.42}$$

and $\hat{\mathbf{u}}_T$ is the unit vector in the direction of the homogeneous solution $\dot{\Theta}_{\mathbf{h},R}$, and

is given by

$$\dot{\Theta}_{\mathbf{h},R} = \begin{bmatrix} \mathbf{I}^{(1\times1)} \\ -\left[\mathbf{J}_1^{(2\times2)}\right]^{-1} \mathbf{J}_0^{(2\times1)} \end{bmatrix}. \tag{3.43}$$

A comparison of the two Jacobians $\mathbf{J_R}$ and $\mathbf{J_T}$, reveals that the Jacobian $\mathbf{J_R}$ is simpler and as a result relatively less computation time will be required for the representation in Cylindrical coordinates as compared to Cartesian coordinates.

3.4.3 Inclusion of Power Limitation

As mentioned previously, the movement of joints that does not contribute to any end-effector motion is referred to as 'self motion'. In the case of redundant links, the calculated joint solution includes the joint motions required to move the end-effector as well as the self joint motion. The self motion can be scaled up or down without affecting the end-effector trajectory. A scaling factor k can be used to maximize the optimization effect.

Euler *et al.* (1988) introduced a method to calculate the appropriate value of k based on bounds of joint velocities introduced by hardware. k_{max} and k_{min} are calculated as following:

$$k_{max_i} = \max\left(\frac{\dot{\Theta}_{max_i} - \dot{\Theta}_{p_i}}{\dot{\Theta}_{h_i}}, \frac{-\dot{\Theta}_{max_i} - \dot{\Theta}_{p_i}}{\dot{\Theta}_{h_i}}\right) \tag{3.44}$$

$$k_{min_i} = \min\left(\frac{\dot{\Theta}_{max_i} - \dot{\Theta}_{p_i}}{\dot{\Theta}_{h_i}}, \frac{-\dot{\Theta}_{max_i} - \dot{\Theta}_{p_i}}{\dot{\Theta}_{h_i}}\right) \tag{3.45}$$

where $\dot{\Theta}_{max_i}$ is maximum joint velocity for the i_{th} joint, $\dot{\Theta}_{p_i}$ is the particular

solution and $\dot{\Theta}_{h_i}$ is the homogeneous solution (see Equation 3.6). k_{max} and k_{min} can then be selected as:

$$k_{max} = \min\left(k_{max_1}, k_{max_2}, \ldots k_{max_n}\right) ,$$

$$k_{min} = \max\left(k_{min_1}, k_{min_2}, \ldots k_{min_n}\right) .$$

The value of k will be k_{max} for maximization and k_{min} for minimization of the performance criterion $H(\Theta)$.

In heavy-duty machines the hydraulic power demanded by various joints may vary depending on the task. Although these machines are equipped with certain amount of power, it will be beneficial to look at allocating maximum power to those joints required to perform a certain task. For example, the boom requires more hydraulic power than the stick or the extender for the same joint movements. The maximum achievable joint velocities are therefore dependent on the loading and the required number of simultaneous joint motions for performing the desired task. If only one or two joints are engaged, all the power can be utilized to activate these two links and higher joint velocities can be achieved; whereas, if all four joints are engaged, the power will be distributed amongst these four joints and lower joint velocities may be the result. Thus, the commanded joint speeds may not be achievable as the result of these constraints and the joint velocity limits need to be calculated and updated.

In the case of coordinated-motion control when high end-effector speed are required, the direction of the end-effector velocity is given importance rather than its magnitude. For example, when the operator fully deflects the joystick, his in-

tention is to achieve the highest possible end-effector velocities in the commanded direction at that particular instance.

Depending upon the total hydraulic power available, Sepehri (1990) proposed an algorithm which determines in advance, whether the joint velocities specified for a motion are achievable or not. The scheme takes into account that in hydraulically actuated manipulators, each joint velocity can be related to the hydraulic oil flow directed to its actuator. Using this approximation, the desired oil flow rates from the main line to the corresponding actuators are first calculated based on the desired joint velocities. These desired flow rates are then checked against the maximum available flow rates from the pumps. Any violations should be modified by equally scaling down all the desired joint velocities. The desired path is still obtained but at a lower velocity.

The above procedure provides a scaling factor ρ. $\rho > 1$ means the desired joint velocities are achievable and the extra power available can be used to optimize some performance criteria. $\rho < 1$ means the desired joint velocities are not achievable and should be scaled down. Multiplication of ρ with desired joint velocities will give the maximum achievable joint velocities.

Let $\dot{\Theta}_p$ and $\dot{\Theta}_h$ be the particular and homogeneous solutions as given in Equation (3.6). $\dot{\Theta}_p$ is the required motion of joints necessary to achieve the end-effector velocity and $\dot{\Theta}_h$ is the self motion. The minimum-norm, least squares solution $\dot{\Theta}_{MN}$ can be calculated from $\dot{\Theta}_p$ and $\dot{\Theta}_h$ as outlined in Equation (3.15). This solution is used as the desired velocity to determine the scalar factor ρ. $\rho\dot{\Theta}_{MN}$ is the maximum joint velocities that can be achieved without any joint

limit avoidance.

A factor β is now introduced to control the optimization effect. For example a value of $\beta = 0.2$ indicates that at least 20% of the achievable joint velocities should be used for joint limit avoidance purposes and the rest for actually moving the end-effector. k can then be calculated based on β and ρ.

Let k_{max} and k_{min} be the upper and lower limits on the scalar constant k, such that the joint velocities for all the joints are within bounds. Three cases may result:

Case 1: $\rho \geq 1 + \beta$,

which means that only fraction of the total available power is required to perform the actual task and that the required end-effector velocities are easily achievable. In this case, k_{max_i} and k_{min_i} are determined to maximize the joint limit avoidance capability:

$$k_{max_i} = \max\left(\frac{\dot{\Theta}_{max_i} - \dot{\Theta}_{MN_i}}{\dot{\Theta}_{H_i}}, \frac{-\dot{\Theta}_{max_i} - \dot{\Theta}_{MN_i}}{\dot{\Theta}_{H_i}}\right) \tag{3.46}$$

and

$$k_{min_i} = \min\left(\frac{\dot{\Theta}_{max_i} - \dot{\Theta}_{MN_i}}{\dot{\Theta}_{H_i}}, \frac{-\dot{\Theta}_{max_i} - \dot{\Theta}_{MN_i}}{\dot{\Theta}_{H_i}}\right) \tag{3.47}$$

where $\dot{\Theta}_{max_i} = \rho\,\dot{\Theta}_{MN_i}$ and $\dot{\Theta}_{H_i} = \left(\nabla H^T\,\hat{\mathbf{u}}_s\right)\,\hat{\mathbf{u}}_s$ (see Equation 3.18). The desired end-effector velocity is achieved along with the maximum optimization (more or equal to the desired level of β).

Case 2: $\rho < 1 + \beta$,

showing that both the required end-effector velocities and the optimization

(β) are not achievable. In this case, the required end-effector velocity is reduced by $(\rho - \beta)$. For example, given $\beta = 0.2$ (20%) and $\rho = 1.1$, in order to keep the desired level of optimization (*i.e.*, $\beta = 0.2$) the required end effector velocities needs to be reduced by $(\rho - \beta = 0.9)$. k_{max_i} and k_{min_i} are therefore determined as follows:

$$k_{max_i} = \max\left(\frac{\dot{\Theta}_{max_i} - (\rho - \beta)\dot{\Theta}_{MN_i}}{\dot{\Theta}_{H_i}}, \frac{-\dot{\Theta}_{max_i} - (\rho - \beta)\dot{\Theta}_{MN_i}}{\dot{\Theta}_{H_i}}\right) \quad (3.48)$$

and

$$k_{min_i} = \min\left(\frac{\dot{\Theta}_{max_i} - (\rho - \beta)\dot{\Theta}_{MN_i}}{\dot{\Theta}_{H_i}}, \frac{-\dot{\Theta}_{max_i} - (\rho - \beta)\dot{\Theta}_{MN_i}}{\dot{\Theta}_{H_i}}\right) \quad (3.49)$$

Case 3: $\rho < \beta$,

which indicates that the required optimization can't be achieved. In this case, the required end-effector velocity is reduced by ρ and optimization is reduced to zero. As an example, suppose $\beta = 0.2$ (20%) and $\rho = 0.1$, which is even less than the required optimization level β. In such a case the required end-effector velocities are scaled down by $\rho = 0.1$ and k is set to zero.

This scheme is non-iterative, hence is fast and can be used for real-time applications.

3.4.4 Scaling Relative Movements

Referring to Section 3.3, the gradient of H in Equation (3.4) is a vector given by

$$\nabla H = \left[\frac{\partial H}{\partial \theta_1} \quad \frac{\partial H}{\partial \theta_2} \quad \frac{\partial H}{\partial \theta_3} \quad \frac{\partial H}{\partial \theta_4}\right]^T , \tag{3.50}$$

A weighing factor α_i can further be introduced in this equation to offer more control over the individual joints as follows (Zghal, 1990):

$$\nabla H = \left[\alpha_1\frac{\partial H}{\partial \theta_1} \quad \alpha_2\frac{\partial H}{\partial \theta_2} \quad \alpha_3\frac{\partial H}{\partial \theta_3} \quad \alpha_4\frac{\partial H}{\partial \theta_4}\right]^T , \tag{3.51}$$

Assigning equal values for α_i (for example $\alpha_i = 1$ for $i = 1, 2, \ldots, n$), gives equal weights to all the joints. In such a case, for a specific end-effector velocity all the joints are likely to move equally and their movement is only dependent upon their current status (*i.e.,* joint position within the joint limits) as well as on the performance criterion utilized. A relatively high value of α_i makes the joint less likely to move, keeping the joint in the mid range. If one considers the coordinated-motion control of heavy-duty machines, the parameter α_i can be used for the following cases:

Case 1: As compared to other links, "boom" is a heavy link; its rapid movements may generate undesirable reactions leading to machine's instability. By assigning a relatively high value of α, as compared to other joints, the movement of the boom can be minimized. In this case the machine is more likely to use the other joints to achieve the desired end-effector velocity. "Boom" will only be used if its use is absolutely necessary.

Case 2: The machine mobility can also be introduced in the inverse kinematic solution as an additional degree-of-freedom ('forward/backward' or 'left/right' motion). Assigning a comparatively high value to the corresponding α, will allow the machine to move 'forward/backward' or 'left/right' only if it is absolutely necessary. An example would be when the target point is outside the work envelop of the machine.

CHAPTER 4

SIMULATION STUDIES

Details of simulation studies conducted to validate the formulation of the inverse kinematic solution are presented in this chapter. Section 4.1 presents the joint limit avoidance capabilities of the scheme when applied to the Spyder machine (shown in Figure 2.1). Section 4.2 compares the results from simulation studies with experimental data. The experimental data was previously collected from an instrumented Caterpillar 215B excavator. Section 4.3 demonstrates the effectiveness of the developed joint-limit avoidance criterion when compared to other performance criteria. Section 4.4 describes the capabilities of the new joint avoidance performance criterion and finally Section 4.5 includes a scheme to improve the control over individual joint motions.

Figure 4.1 shows the developed PC-based simulator. It utilizes a three degree-of-freedom joystick interfaced to a PC-486, 33Mhz computer through a DAS-16 analogue to digital conversion card. The joystick produces a voltage signal (0-12volt) proportional to the deflection of the joystick from the mid-position (in the three principal X, Y and Z directions). These voltages are then converted from analogue to digital format by the A/D conversion board. The converted digital numbers which represent the required end-effector velocity, are input to the simulation program. The simulation program (written in C) utilizes the inverse kinematic scheme formulated in Chapter 3 in order to calculate the joint motions.

The graphic module of the simulator displays joint positions, velocities and end-effector position and also provides 3D animation of the machine.

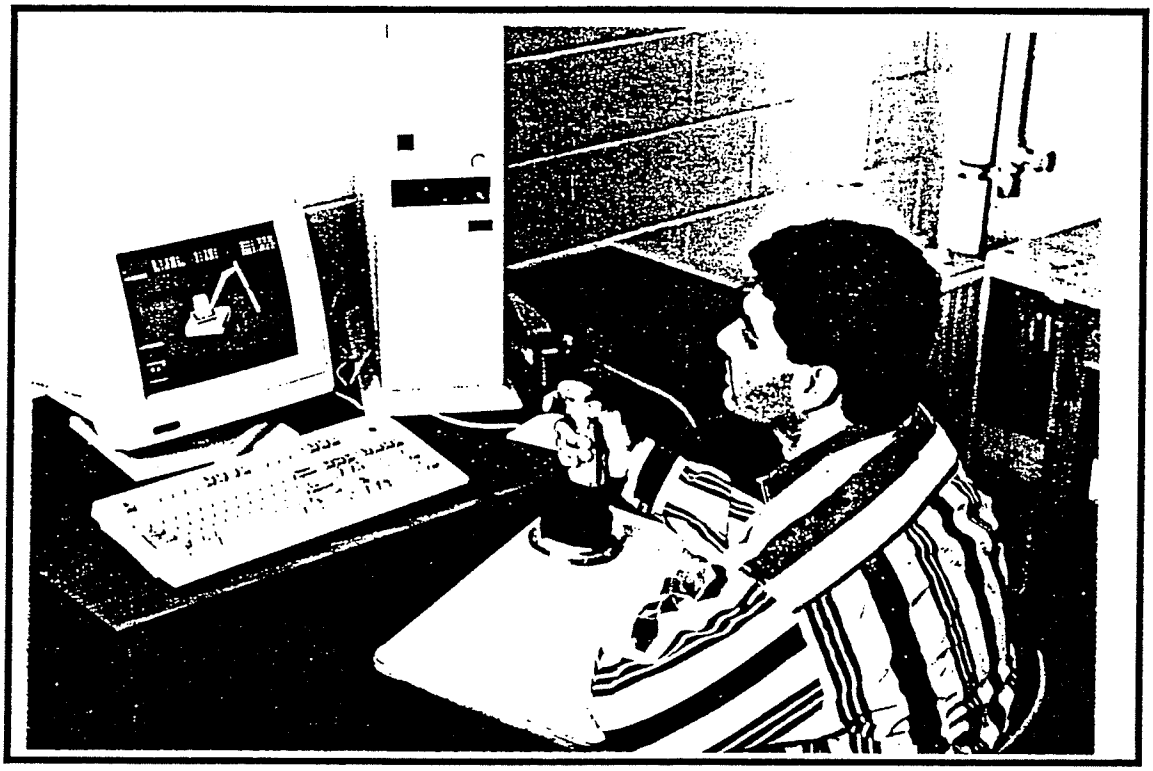

Figure 4.1: PC-based simulator

4.1 Joint Limit Avoidance

This section discusses the effectiveness of the joint limit avoidance criterion developed. The four-degree-of-freedom Spyder machine shown in Figure 2.1 with the link parameters as listed in Table 4.1 was modeled. A simulation is performed by having the end-effector follow an arbitrary trajectory made of straight-line segments. The end-effector tracks such trajectories at constant velocity with ac-

Table 4.1: Kinematic parameters of Spyder

Joint No.	Link name	Min. joint limit	Max. joint limit	Link Length
1	Swing	$-180°$	$180°$	
2	Boom	$-20°$	$60°$	2.8m
3	Stick	$-145°$	$-45°$	1.4m
4	Extender	0.1m	1.1m	0.6 ± 0.5m

accelerating and decelerating segments at the beginning and at the end of each path segment, respectively. The acceleration and deceleration pattern was similar to the one presented by Paul (1981). With reference to Figure 4.2, the simulated work cycle is as follows:

1. The end-effector starts from a home position and moves to position 1. This position represents the beginning of a scraping cycle.

2. The end-effector then moves horizontally towards position 2 close to the base to simulate the scraping motion.

3. At the end of operation 2, when the bucket is full, the end-effector extends to a "dump position" represented by position 3. End-effector stays for approximately six seconds at "dump position" simulating the dumping operation.

4. The final step is to retract the implement (empty bucket) to the staring position (position 1).

Each segment lasts 6 seconds bringing the total task time to 30 seconds. Positions 1 and 2 are chosen to be close to the boundary of the work envelope of the manipulator. These positions were chosen purposely to evaluate the joint

limit avoidance capability of different performance criteria when the joints are subjected to extreme motions.

Figure 4.3 shows the end-effector position (in Cartesian coordinates). Figure 4.4 shows the end-effector velocity generated during the task. The end-effector

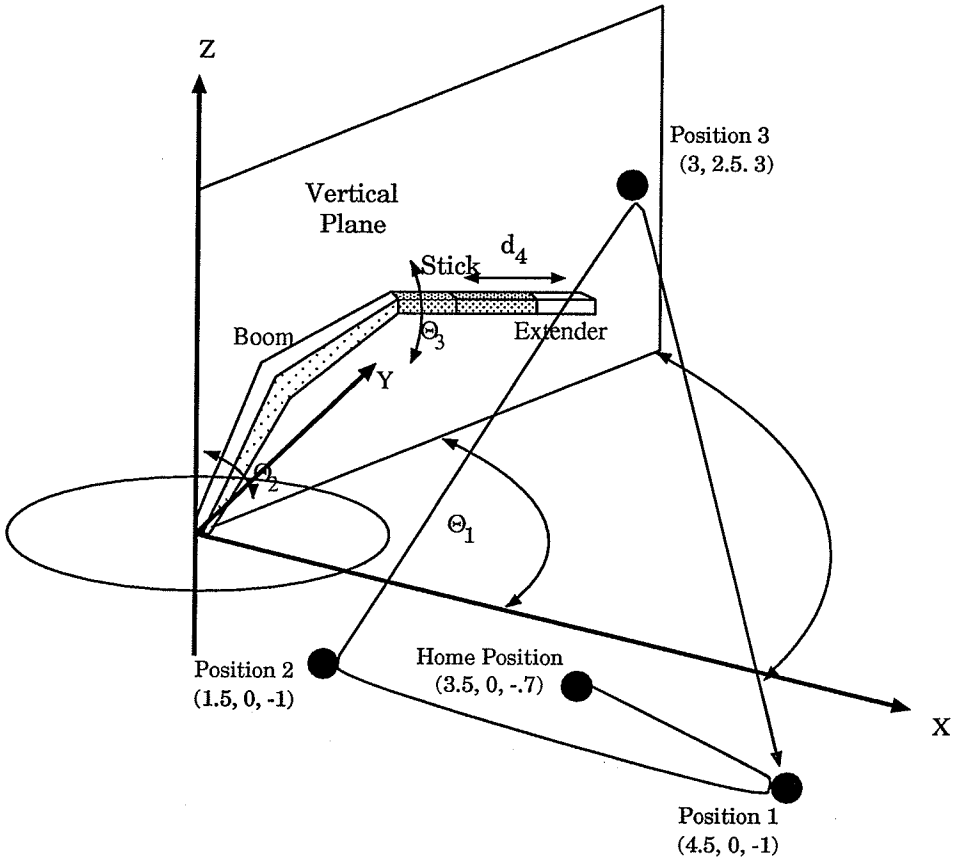

Figure 4.2: Typical excavation duty cycle.

velocity depends upon the distance between two positions *i.e.*, the time allowed to cover that distance and the acceleration time factor. The accelerating/decelerating time factor determines the acceleration/deceleration period. It was arbitrarily chosen as 0.2 times the travel time for each segment. The end-effector velocity profile mimics an ideal joystick command input and therefore was used in the

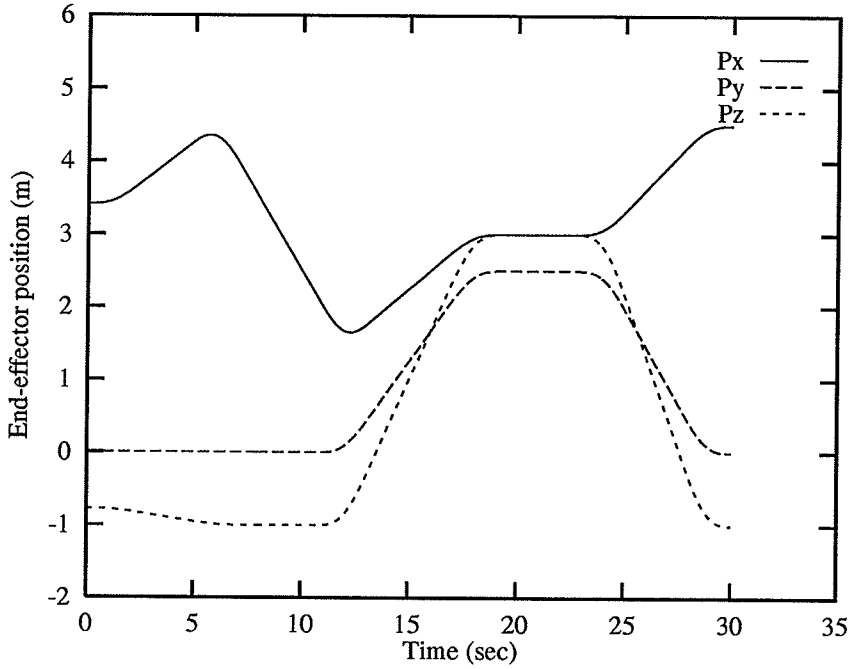

Figure 4.3: End-effector position in a typical duty cycle.

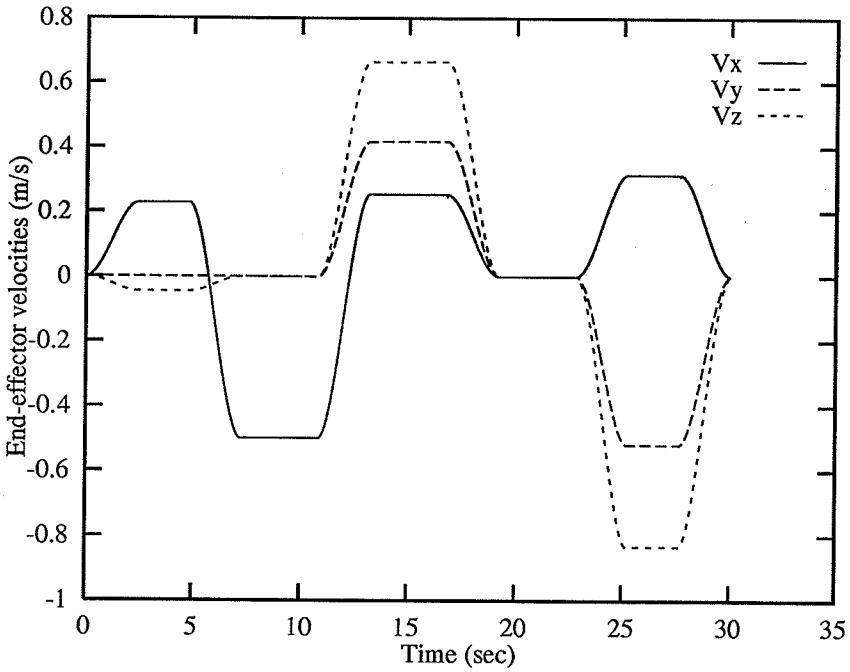

Figure 4.4: End-effector velocity.

inverse kinematic program to solve for the required joint velocities.

All the four performance criteria (H_1, H_2, H_3 and H_4 discussed in Section 3.3) for joint limit avoidance were tested for the above selected path. In this section we only present the results obtained using the joint limit avoidance criterion H_4. The results for other criteria will be presented later in Section 4.3.

The angular joint velocities and displacements for swing, boom, stick and extender are shown in Figures 4.5, 4.6 4.7 and 4.8 shows the linear velocity and displacements of the extender. The gradually changing joint velocities produced low levels of acceleration and velocities which are well within the normal range of operation, as will be shown later with comparison to the actual machine operation in Section 4.2. Other simulation studies also proved that the scheme generates smooth joint motions for any end-effector velocity. Smooth joint motions are expected to contribute to operator's comfort as well as prolong the life of the machine. It is seen that all the joints during the task remained within their bounds (see Table 4.1), even though the end-effector moved to extreme positions. For example, referring to Figure 4.6, near $t = 15$ sec. the compensatory motion in redundant joints were successfully utilized to prevent joint 2 from reaching its joint limit of 60°.

On a 486-33MHz PC, with a sampling frequency of 50Hz the program ran at 50% of the real time speed without any graphic output. The program was also run at the Telerobotic Laboratory at UBC on the flight simulator with faster graphics. The scheme proved to be robust and the results which included the interaction with the human operator were satisfactory. While performing some

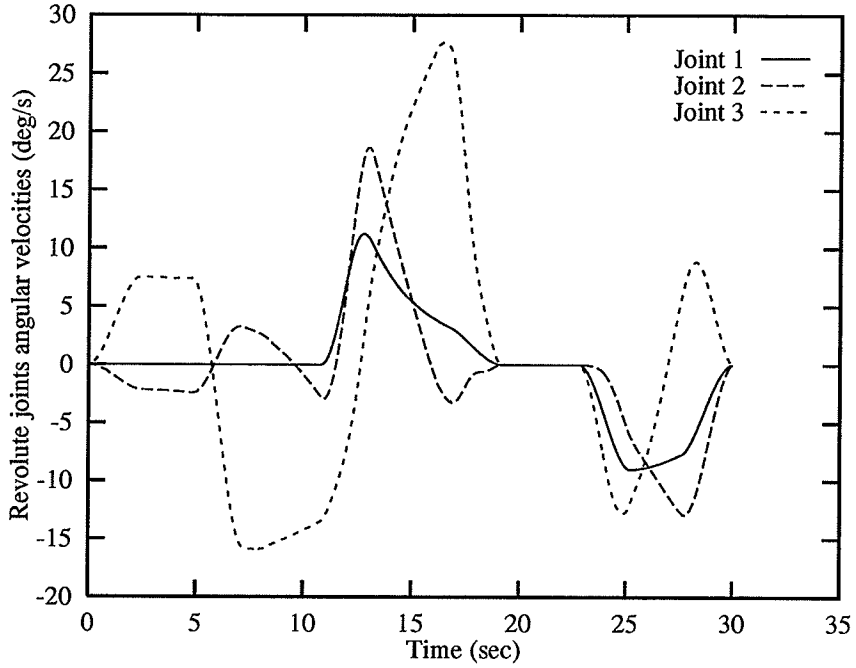

Figure 4.5: Revolute joint velocities (H_4 Criterion).

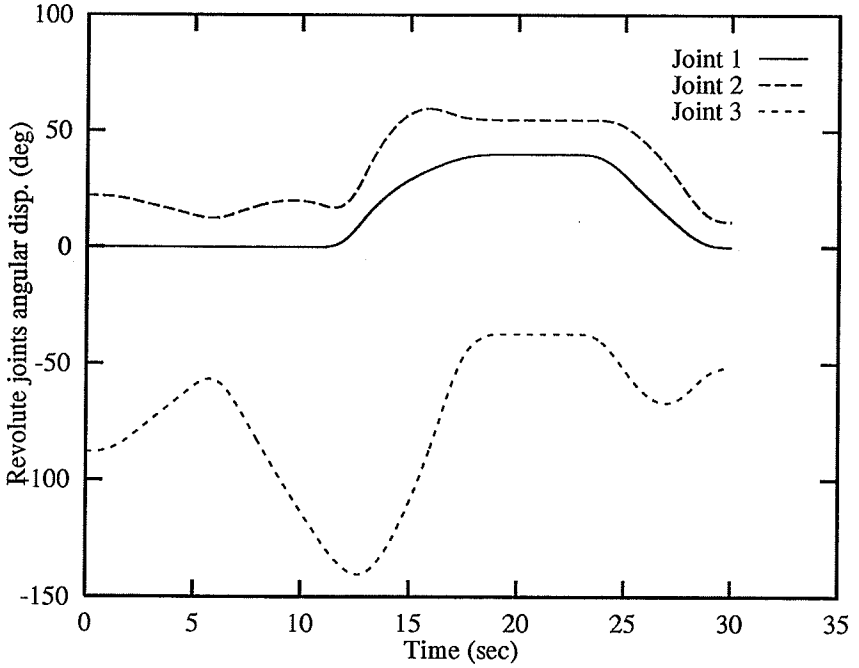

Figure 4.6: Revolute joint displacements (H_4 Criterion).

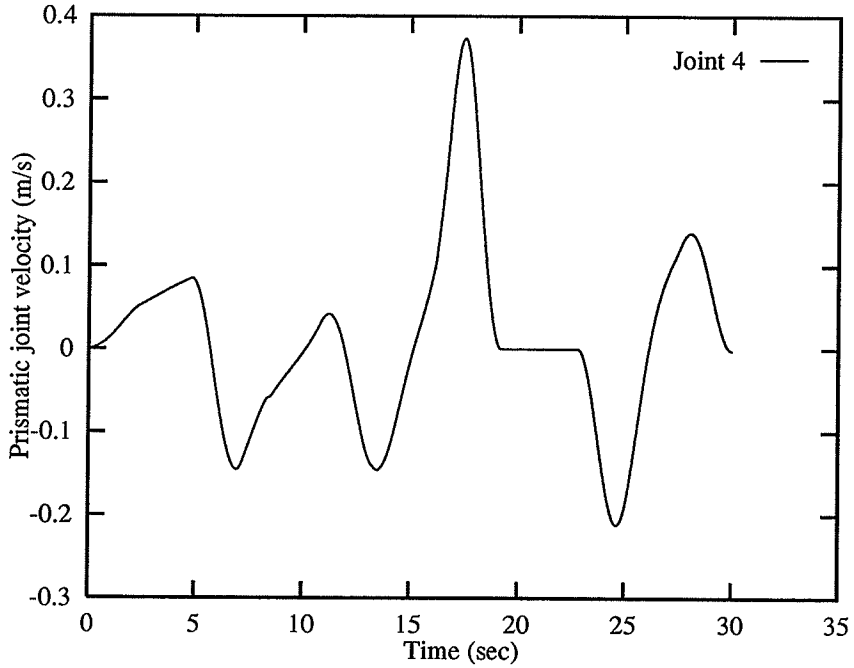

Figure 4.7: Extender velocity (H_4 Criterion).

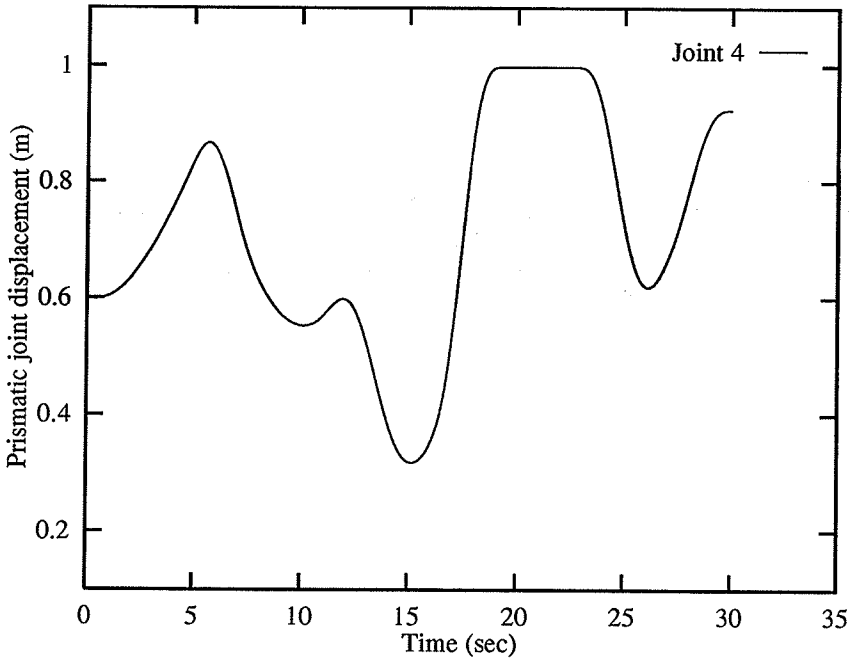

Figure 4.8: Extender displacement (H_4 Criterion).

tasks such as moving the log, the operator successfully avoided the joint limits using the proposed scheme in real-time.

4.2 Comparison to Experimental Results

In this section data obtained from experimental studies are compared with those from simulation. The objective was to compare the joint motions generated by the scheme to those produced by an operator for an identical task.

A three degree-of-freedom 215B Caterpillar excavator available at UBC was utilized to provide the experimental data. This is the only fully instrumented, teleoperated heavy-duty machine available in Canada. An operator was asked to perform a specific task on this machine using a joint-mode control. The end-effector moved from a low altitude position close to the Cab to a high altitude position located far away from the cab, before returning to the initial position (shown as path 1-2 in Figure 4.9). The total cycle time for this task was recorded as 15.4 seconds. The joint angles were sampled at 50 Hz. Using these data and the kinematic information of the machine, the end-effector velocity profile was calculated. The velocity data was then filtered to obtain an analogous joystick input to the simulation program. The simulation program used these velocity commands as joystick commands for input to the four degree-of-freedom model of Kaiser machine (shown in Figure 2.1). The output data from the simulator was synchronized to correspond to the time intervals for which experimental data was available

All link parameters for the Caterpillar 215B excavator are given in Table 4.2.

Table 4.2: Kinematic parameters of 215B Caterpillar excavator.

Joint No.	Link name	Min. joint limit	Max. joint limit	Link Length
1	Swing	$-180°$	$180°$	
1a	Offsets(1 and 2)	—	—	0.31m and 0.12m
2	Boom	$-27°$	$45°$	5.19m
3	Stick	$-157°$	$-25°$	1.80m

Table 4.3: Kinematic parameters used for simulator.

Joint No.	Link name	Min. joint limit	Max. joint limit	Link Length
1	Swing	$-180°$	$180°$	
1a	Offsets(a_1 and d_2)	—	—	0.31m and 0.12m
2	Boom	$-27°$	$45°$	5.19m
3	Stick	$-157°$	$-25°$	1.20m
4	Extender	0.1 m	1.1 m	0.6 ± 0.5

The link parameters for the simulation was selected correspondingly. As shown in Figure 2.1, joints 3 and 4 of Spyder are revolute and prismatic, respectively. The length of link 3 is chosen as 1.2m and length of link 4 (prismatic) can vary from 0.1 to 1.1m with the middle position being 0.6m. In comparison, the experimental machine for which data was available was a three degree-of-freedom, non-redundant machine. Link 3 of this manipulator is revolute with a length of 1.8m. Thus, when link 4 of Spyder is in its middle position, it is similar in geometry to the Caterpillar 215B excavator. However, during the simulation studies link 4 was free to move.

Figures 4.10, 4.11, 4.12 and 4.13 compare the experimental and simulation joint velocity trajectories. The swing velocity obtained from simulation shows

good agreement with the experimental swing velocity. The slight difference in swing velocity (Figure 4.10) may be due to the filtering of the end-effector velocity that was input to the simulation program. The difference in the plots for boom and stick velocities (Figures 4.11 and 4.12) are due to the movement of the fourth link which was free to move in the simulation. As is seen in the plots, on an average, the simulation program generated lower joint velocities than the experimental results.

Figures 4.14, 4.15 and 4.16 compare the joint displacements obtained through simulation with those from experimental studies. Referring to Figure 4.15 the simulation resulted in a reduced movement of the boom compared to the experimental data. Similarly the stick movement was less in simulation. The simulation program moved the extender instead, which reduced the movements of the other joints. It can be noted that the swing displacement are similar in both cases. This is due to the fact that redundancy has no effect on the swing joint. All the joints exhibited motion within the joint limits.

Figures 4.18, 4.19 and 4.20 show the resulting end-effector positions from both simulations and experimental studies. The two follow closely.

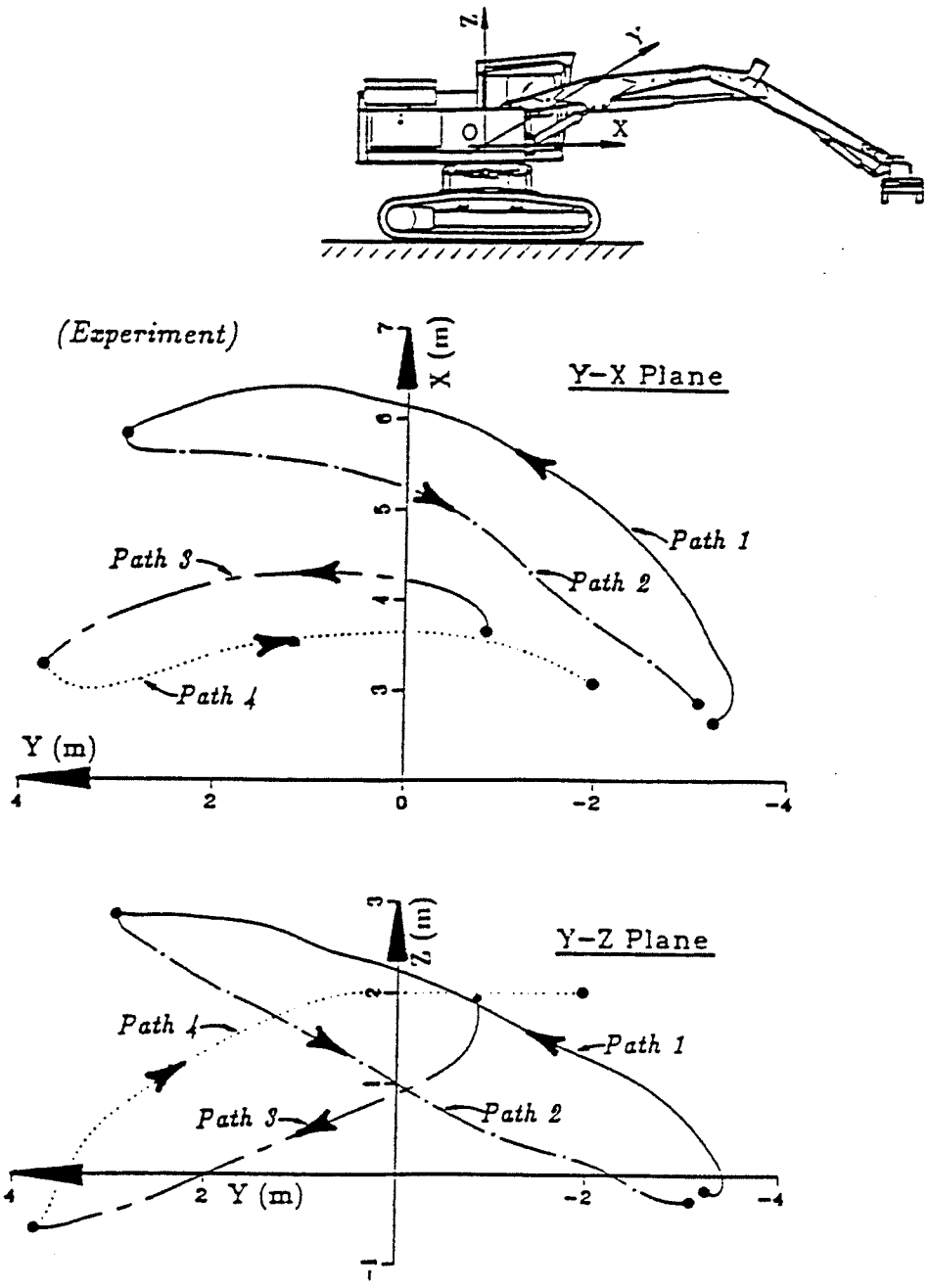

Figure 4.9: Various views of experimental path trajectory

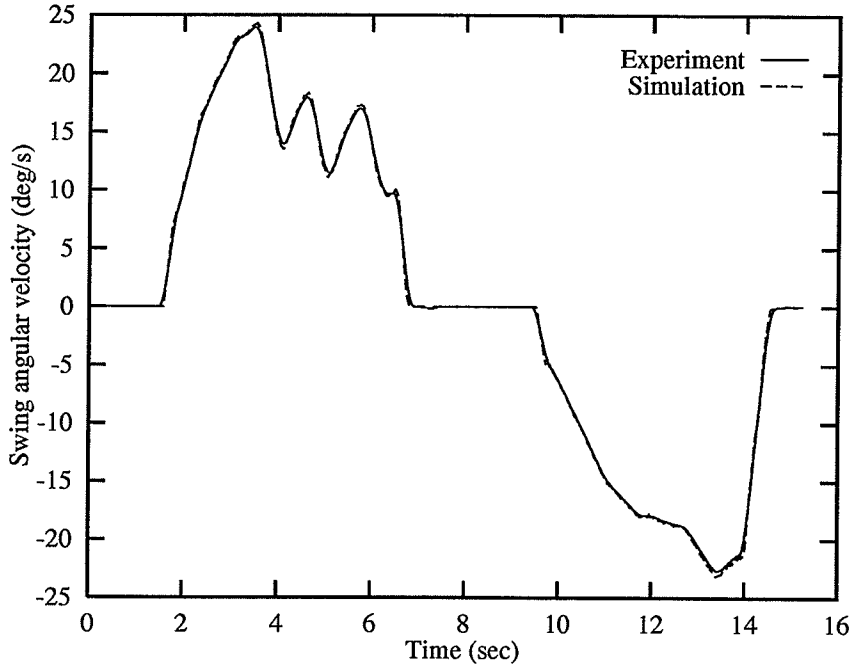

Figure 4.10: Swing velocity (simulation vs. experiment).

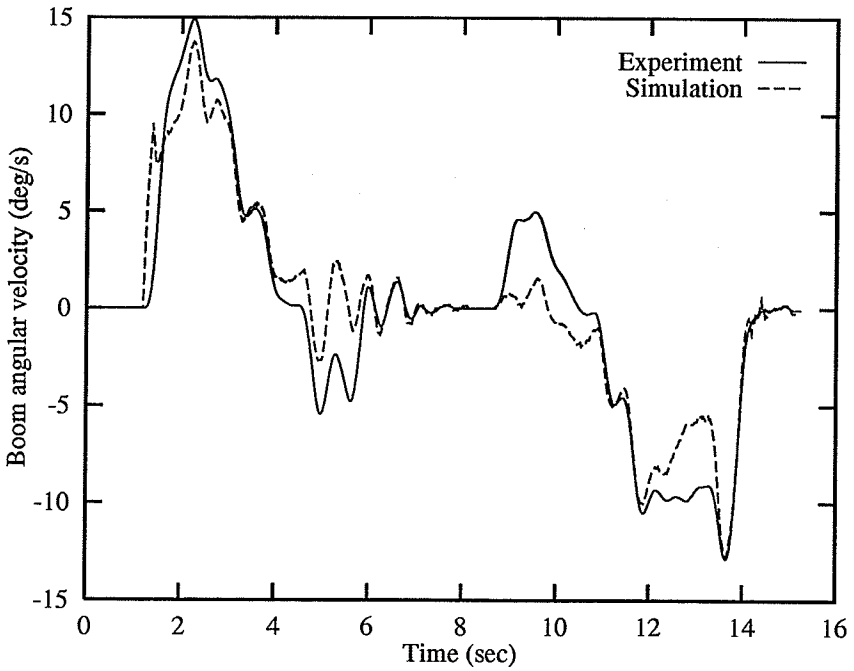

Figure 4.11: Boom velocity (simulation vs. experiment).

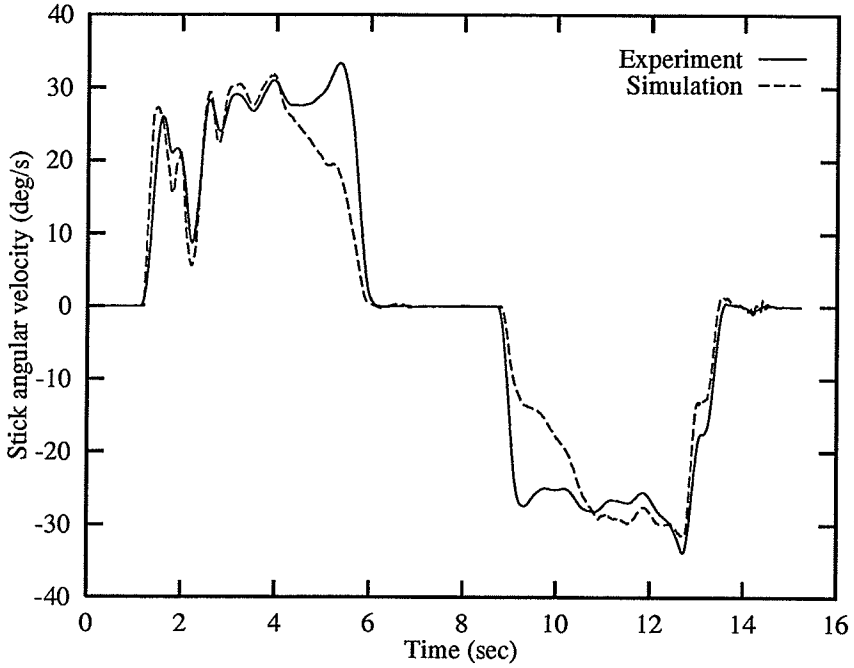

Figure 4.12: Stick velocity (simulation vs. experiment).

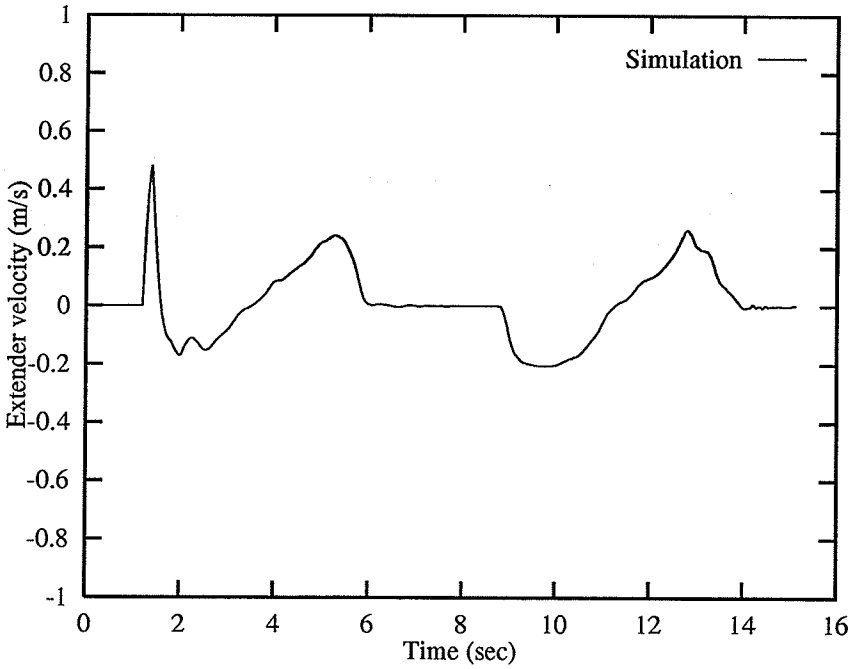

Figure 4.13: Extender velocity (simulation).

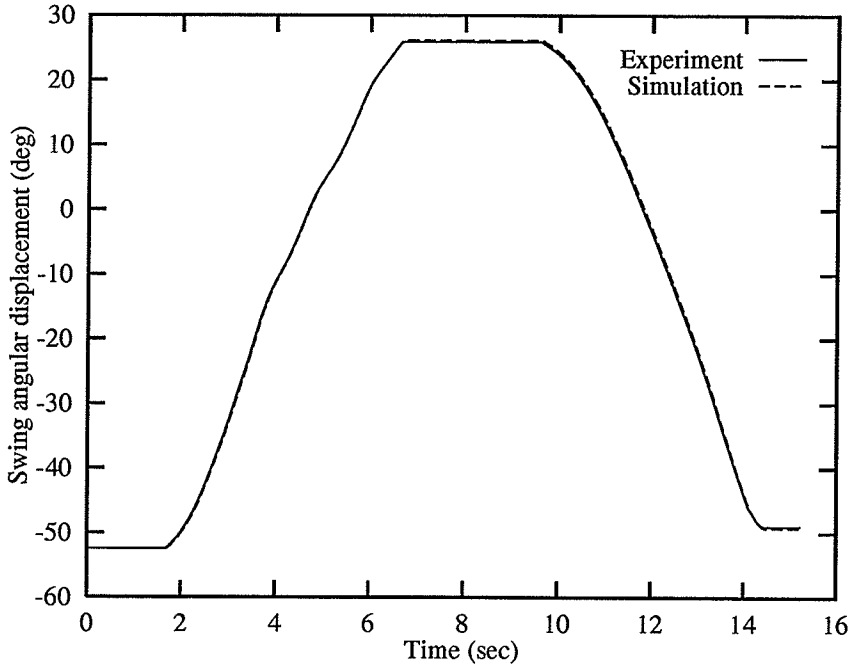

Figure 4.14: Swing displacement (simulation vs. experiment).

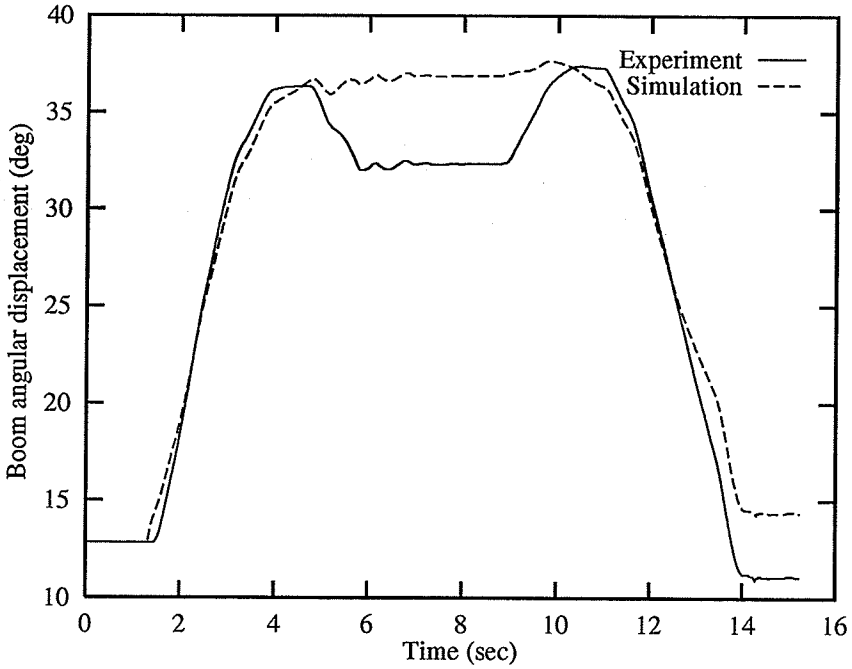

Figure 4.15: Boom displacement (simulation vs. experiment).

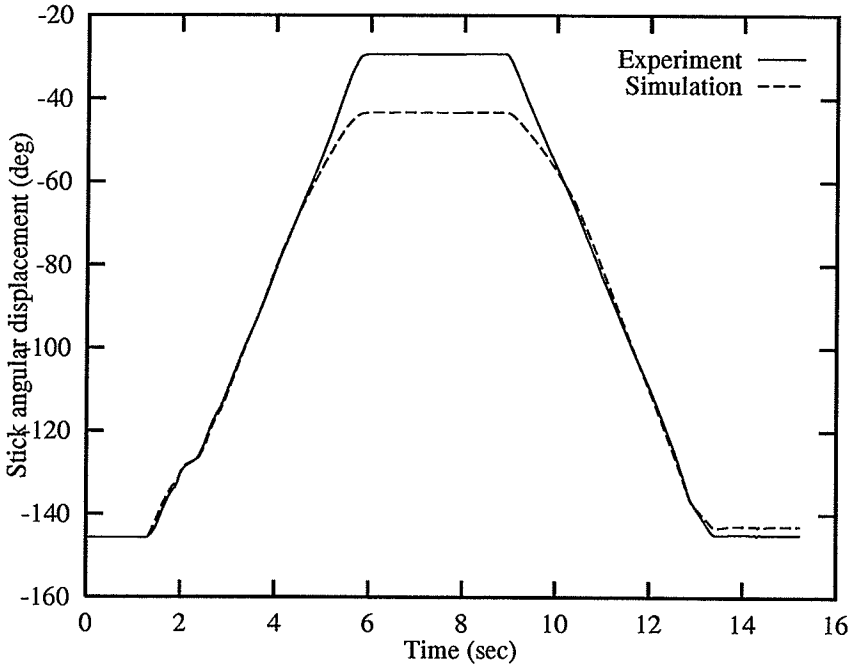

Figure 4.16: Stick displacement (simulation vs. experiment).

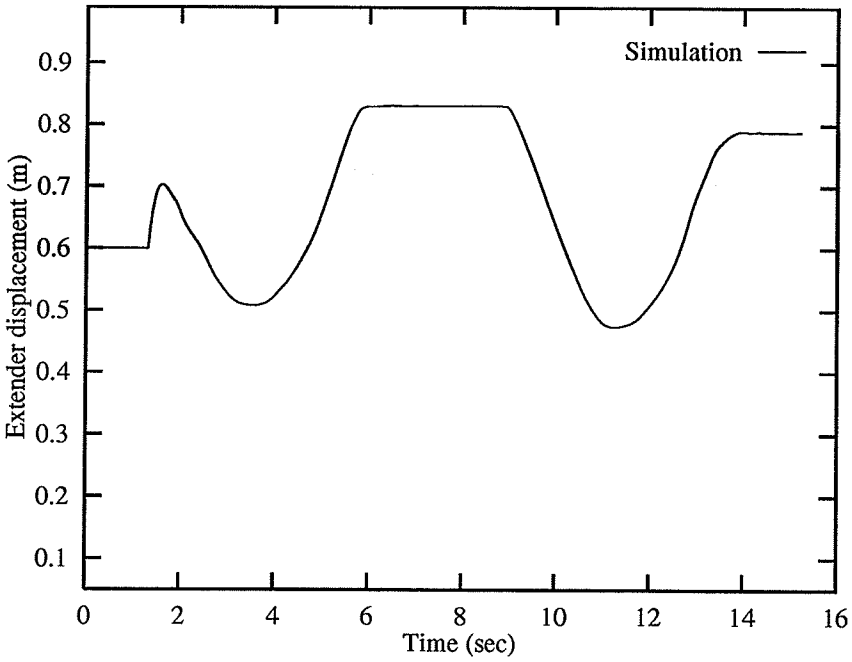

Figure 4.17: Extender displacement (simulation).

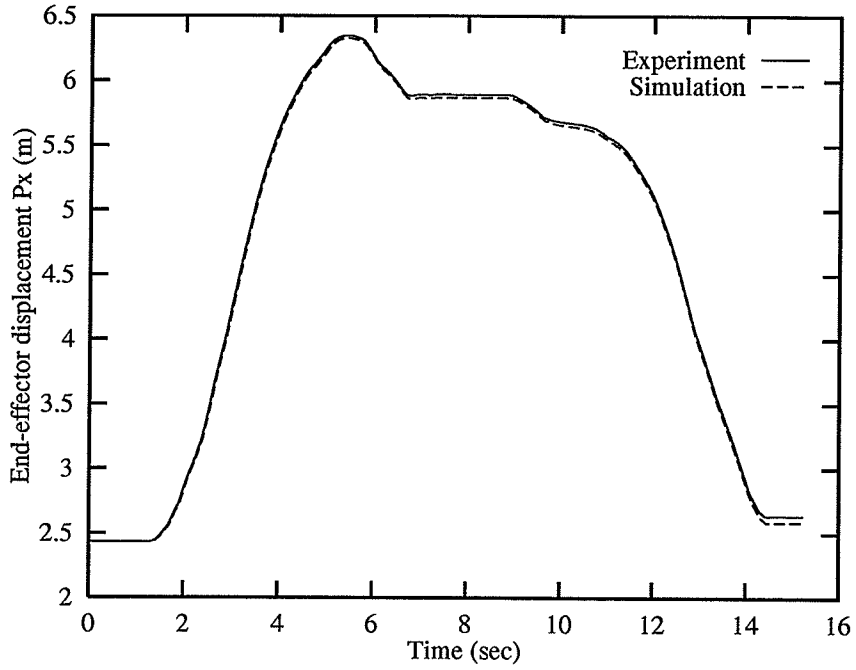

Figure 4.18: End-effector position P_x (simulation vs. experiment).

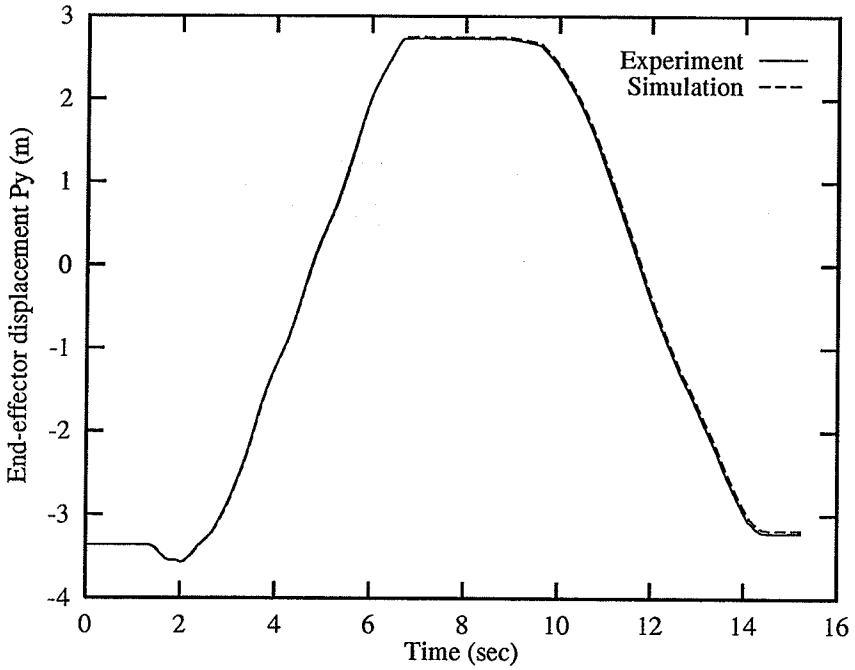

Figure 4.19: End-effector position P_y (simulation vs. experiment).

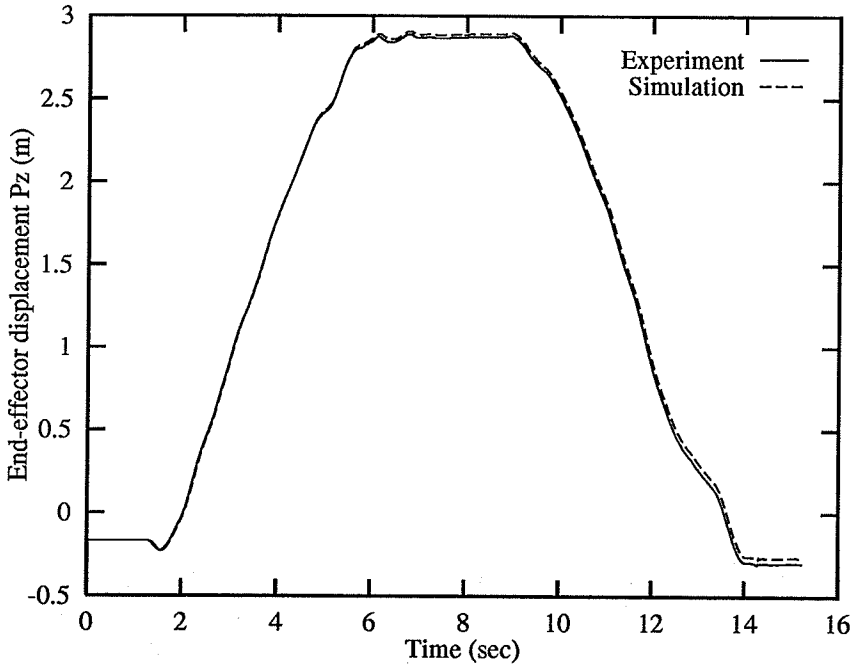

Figure 4.20: End-effector position P_z (simulation vs. experiment).

4.3 Comparison to Other Joint Limit Avoidance Criteria

In this Section the performance of the different criteria H_1, H_2, H_3 and H_4 discussed in Section 3.3 are compared. All the criteria were tested by subjecting them to the same task as outlined in Section 4.1. Figure 4.3 shows the end-effector position and Figure 4.4 shows the end-effector velocity generated during this task. H_1 and H_2 criteria are both linear with H_2 having a higher gradient. Applying the scaling factor k (see Section 3.4.3), H_1 and H_2 will ultimately result in producing the same optimization, thereby producing similar joint motions. As a result only the results obtained for H_1 are included here. Also as already outlined in Sections 4.1 and 4.2, the redundancy of Spyder has no effect on the swing joint motion. Therefore the results for the swing joint are similar for all the cases and hence are not presented.

Figures 4.21, 4.22 and 4.23 show the joint velocities of the Boom, Stick and Extender. Criterion H_1 generated smooth joint velocities but were less capable of avoiding joint limits. On the other hand criterion H_3 effectively avoided joint limits but it generated less smooth joint velocities.

Figure 4.24 shows the motion of the boom for all four criteria. The joint range for the boom (see Table 4.3) is from $-20°$ to $60°$. It is clear from the figure that performance criterion H_1 was not able to avoid the upper joint from reaching its limit. Other two criteria successfully avoided the joint limits. Note that H_1 generates linear gradient and therefore has the least joint limit avoidance capability.

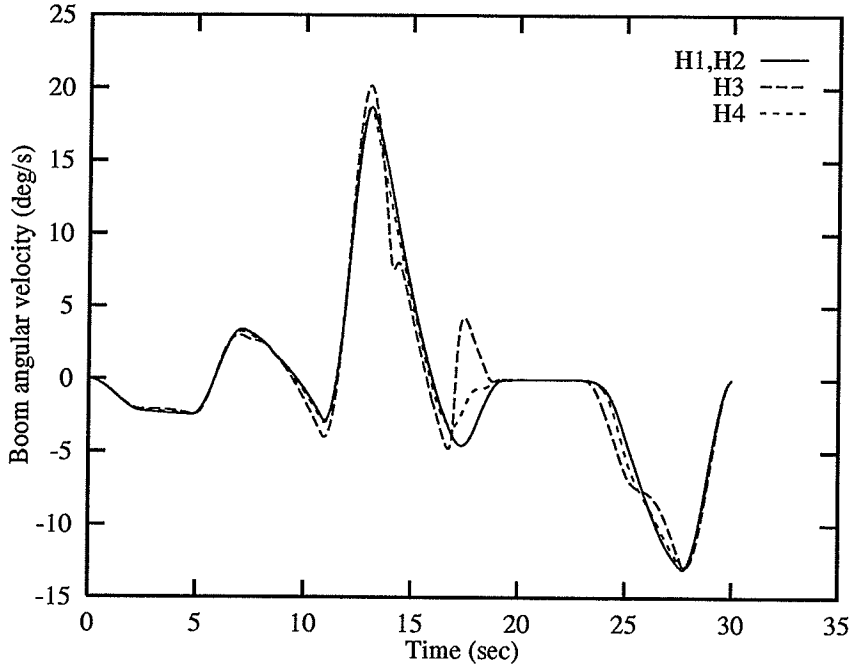

Figure 4.21: Boom angular velocity.

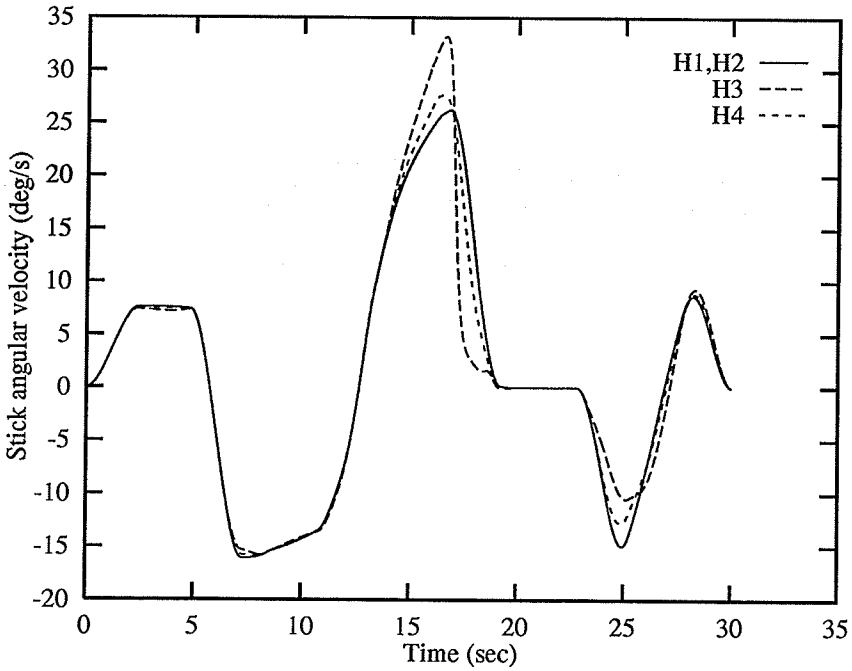

Figure 4.22: Stick angular velocity.

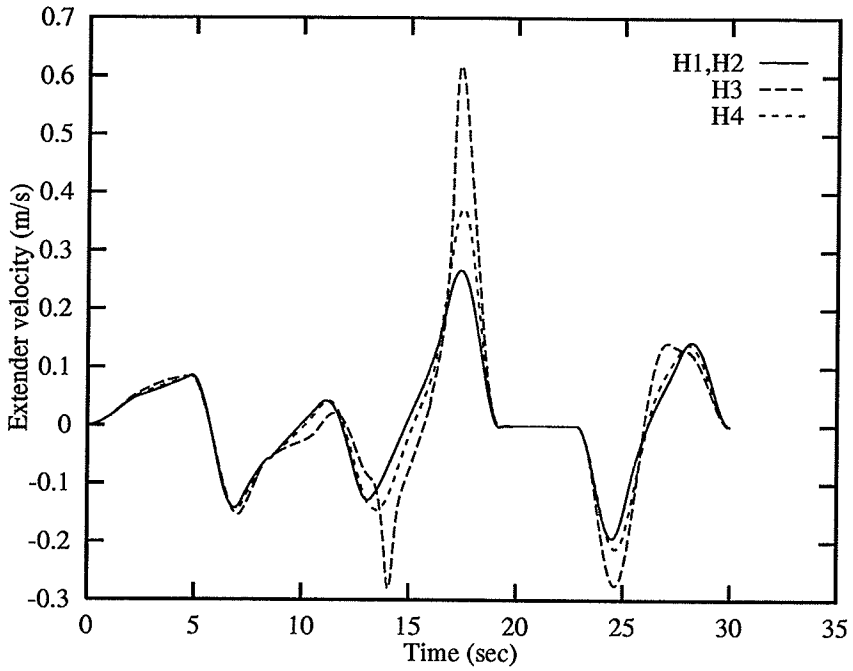

Figure 4.23: Extender linear velocity.

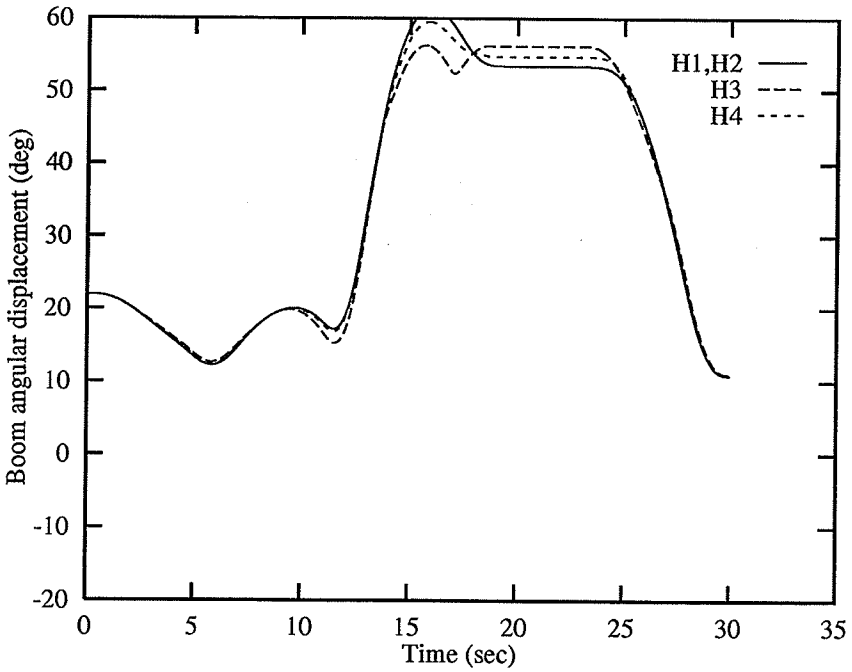

Figure 4.24: Boom displacement.

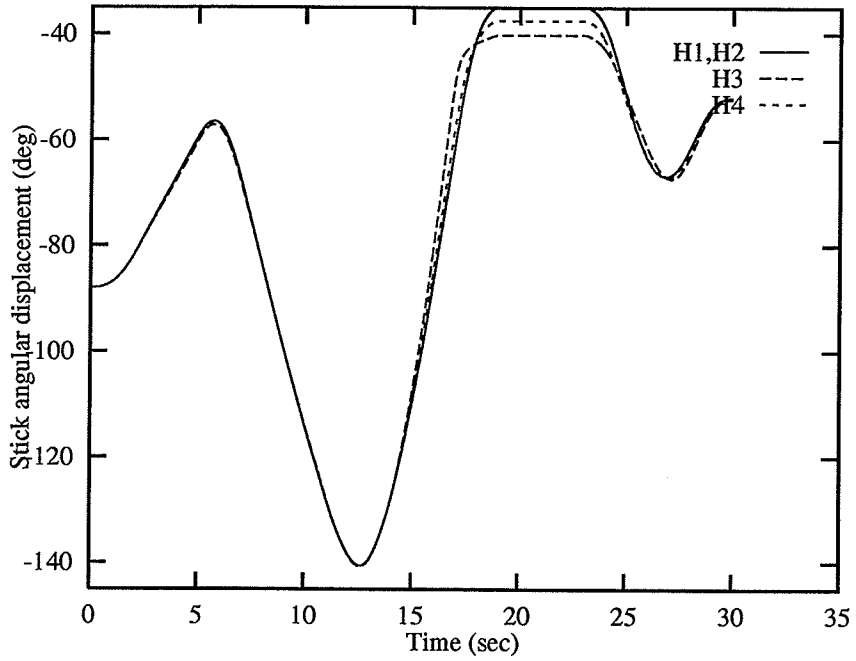

Figure 4.25: Stick displacement.

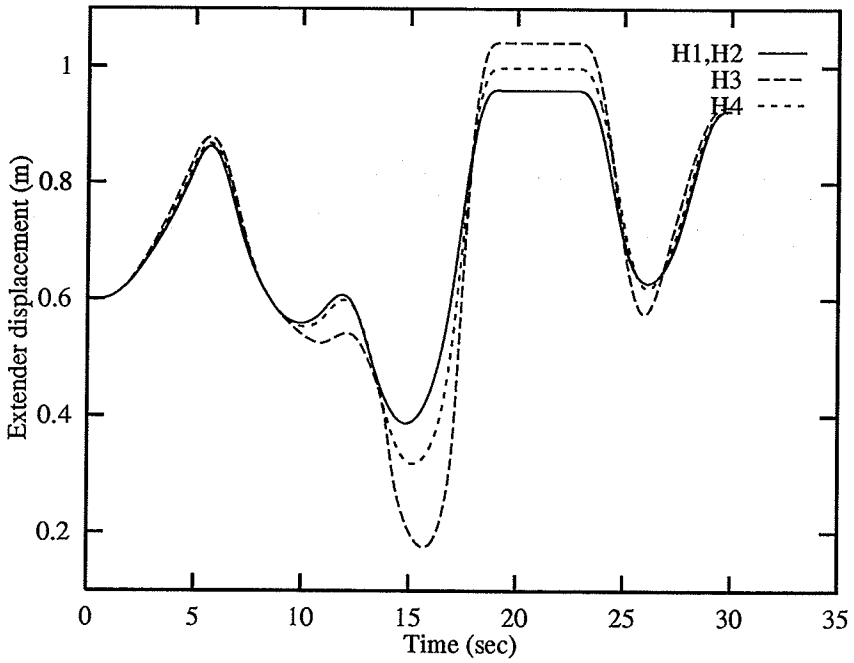

Figure 4.26: Extender displacement.

Figure 4.25 shows the motion of the stick. The joint range for the stick joint is from $-145°$ to $-45°$. Again it is noted that performance criterion H_1 was not able to avoid the upper joint limit. All other criteria successfully avoided the joint limits.

Figure 4.26 shows the motion of the extender. The joint range for the extender is from $0.1m$ to $1.1m$. All performance criteria successfully avoided the joint limits. Criterion H_3 utilized the extender more, in comparison to other performance criteria. Near the 13_th sec. the upward change in the extender motion was to prevent the stick from reaching its joint limit of -140°.

In general criterion H_4 produced smooth joint velocities while preventing the joint limits. In fact, performance criterion H_4 is configurable and can simulate the properties of all the criteria from H_1 to H_3. This will be shown in the next section.

4.4 Effect of (ϕ)

Referring to Equation (3.26), a value of $\phi = 0$ represents no optimization. This is equivalent to the minimum-norm least squares solution outlined in Equation (3.4). A high value of ϕ, for example $\phi \geq 100$ represents a situation when the maximum possible joint limit avoidance can be attained. In order to show the effect of ϕ, an arbitrary path similar to the one discussed in Section 4.1 was simulated, using H_4 criterion and different values of ϕ. The path points were purposely chosen to be very close to workspace boundaries of the Spyder to demonstrate the effect of ϕ.

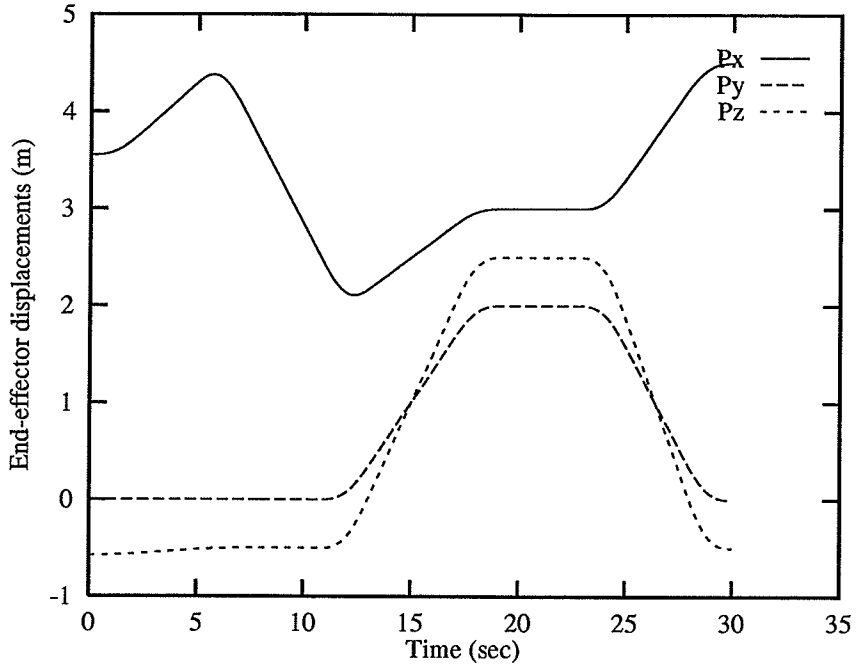

Figure 4.27: End-effector position.

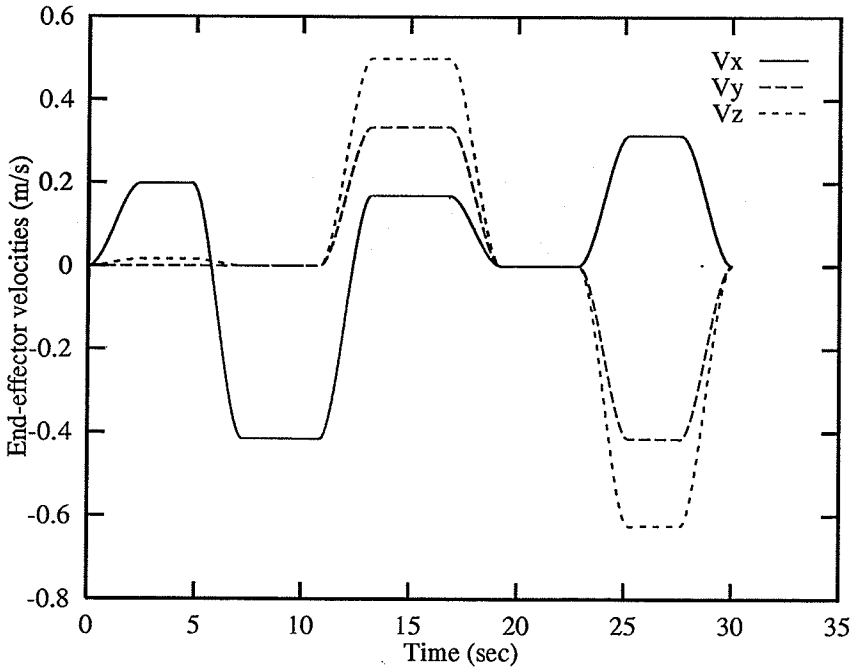

Figure 4.28: End-effector velocity.

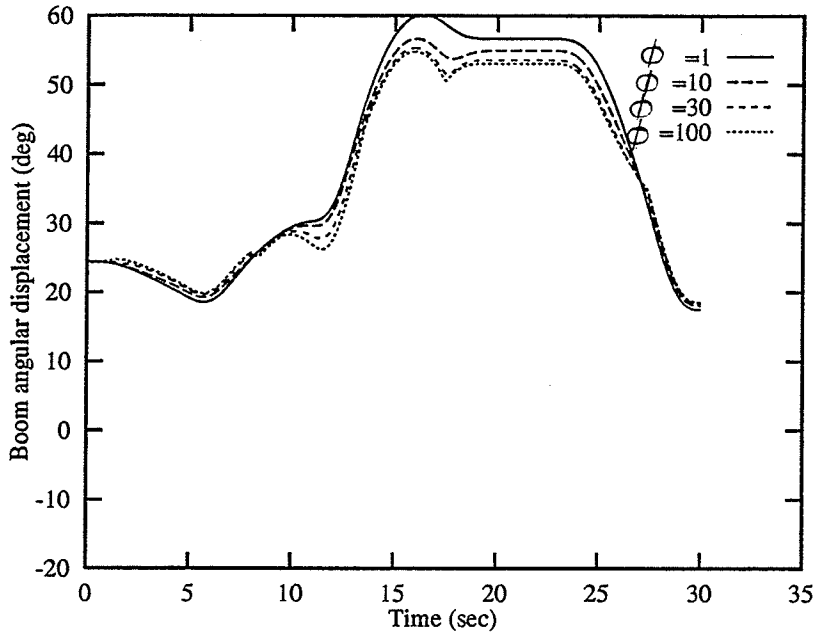

Figure 4.29: Boom displacement for different values of ϕ.

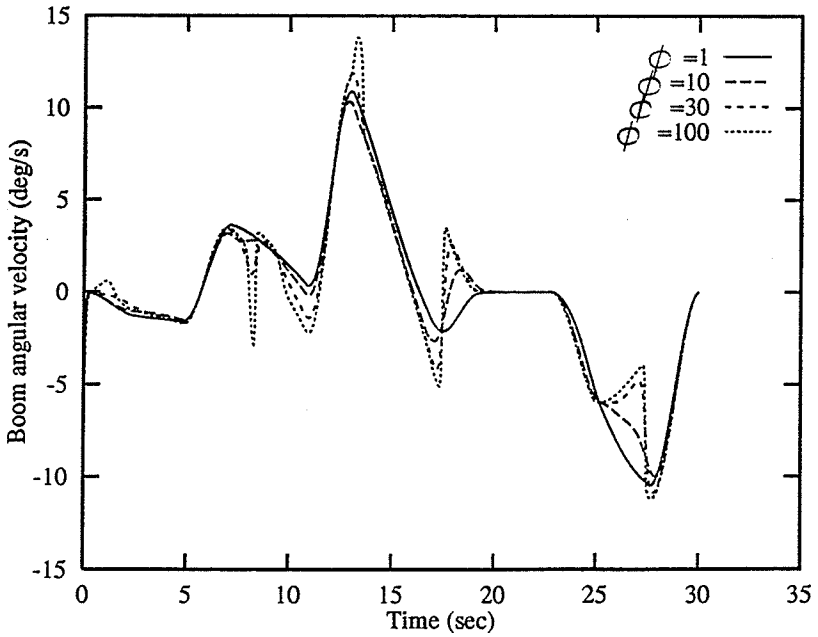

Figure 4.30: Boom angular velocity for different values of ϕ.

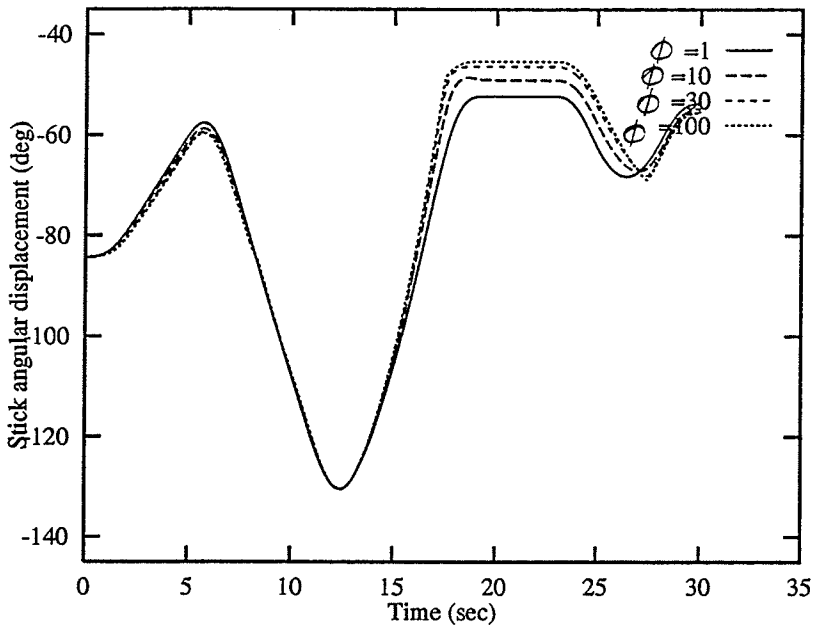

Figure 4.31: Stick displacement for different values of ϕ.

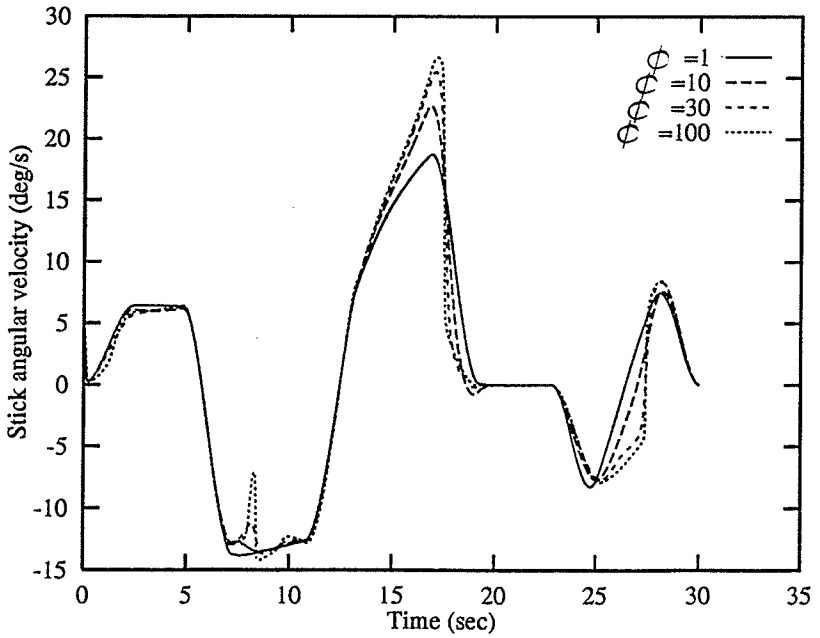

Figure 4.32: Stick angular velocity for different values of ϕ.

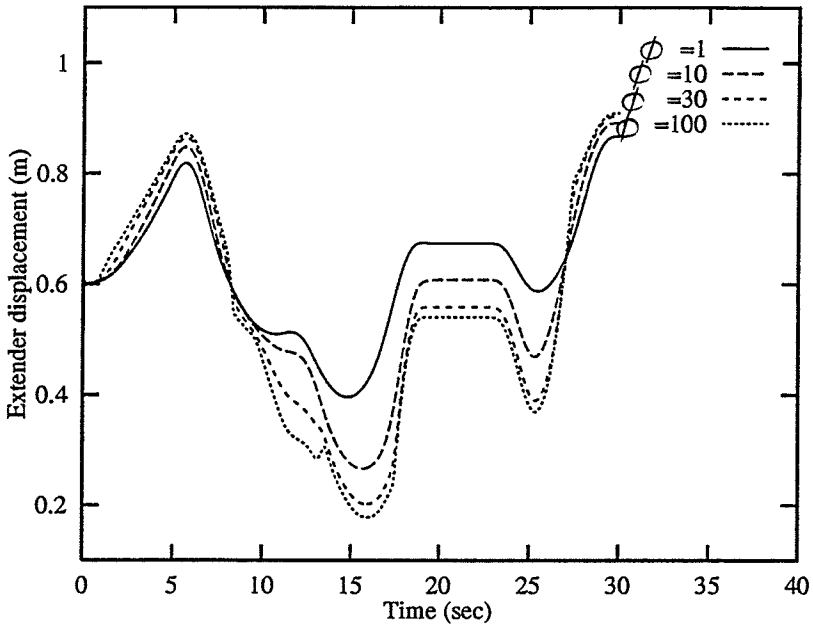

Figure 4.33: Extender displacement for different values of ϕ.

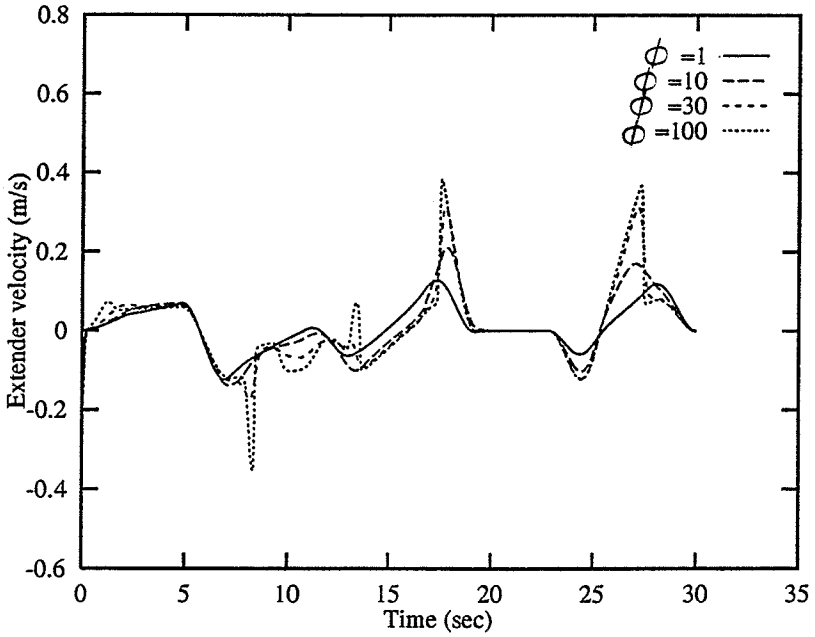

Figure 4.34: Extender velocity for different values of ϕ.

Figures 4.27 and 4.28 show the end-effector position and velocity components for this path. Figures 4.29, 4.31 and 4.33 show the joint displacements for boom, stick and extender, respectively. The joint limit avoidance capability of the criterion at different values of ϕ can be seen from these figures. Smaller ϕ performs better; and does not result in abrupt changes in velocity profile. However very low ϕ would not allow the joint to recover from the joint limit as fast as possible. During the course of this study it was observed that values of $\phi \in [5, 15]$ gave results comparable to experimental observations. A value of $\phi \approx 5$ gave smoother joint velocities while a value of $\phi \approx 15$ increased the joint limit avoidance capability at the expense of greater variation in the velocity profile.

Figures 4.30, 4.32 and 4.34 show the joint velocities for the above case. Considering both joint limit avoidance and the velocity generated, it is clear that, for lower value of ϕ smoother joint velocities are generated.

4.5 Control over Individual Joint Motions (α)

α_i in Equation 3.51 is a weighing factor for joint i. Equal values of α_i (*i.e.* $\alpha_i = 1$) give equal weights to all the joints. In such a case, for a specific end-effector velocity all the joints are likely to move equally and their movement is only dependent upon their current position. A relatively higher value of α_i makes the joint i less likely to move as compared to other joints and keeps the joint near its mid-range.

This section demonstrates the use of α to restrict the relative movement of one or more joints by assigning a relatively high value to the corresponding α. Same task as in Section 4.4 (see Figures 4.27 and 4.28) was used and α_4, for extender joint was changed, keeping the other joints equally mobile (i.e. $\alpha_i = 1$ for $i \neq 4$). Performance criterion H_4 was used with $\phi = 10$. Figures 4.35, 4.37 and 4.39 show the joint displacements for different values of α_4. As seen in Figure 4.39, a higher value of α_4 compared to α_2 and α_3 keeps the extender near the mid-position while a lower value makes the extender more active in contributing to the end-effector positioning. Figures 4.36, 4.38 and 4.40 show the joint velocities for different values of α_4. A higher value of α_4 generated lower and more gradually changing extender velocity.

Any individual link can be made more active or passive by giving a lower or higher value of α_i respectively. The inclusion of this property to the scheme can enhance the stability of the excavators by making the heavier links such as boom, sluggish. This is expected to reduce the effect due to dynamics of moving very

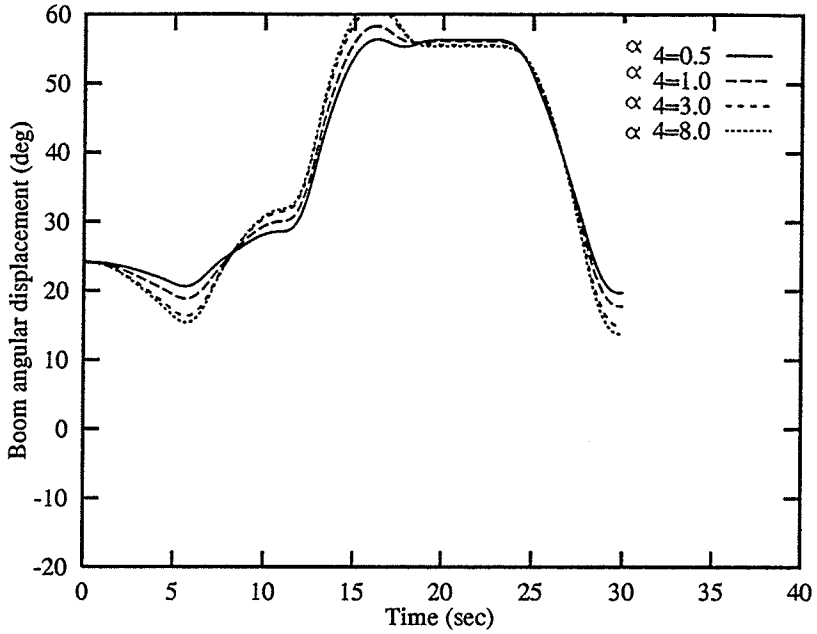

Figure 4.35: Boom displacement for different values of α_4.

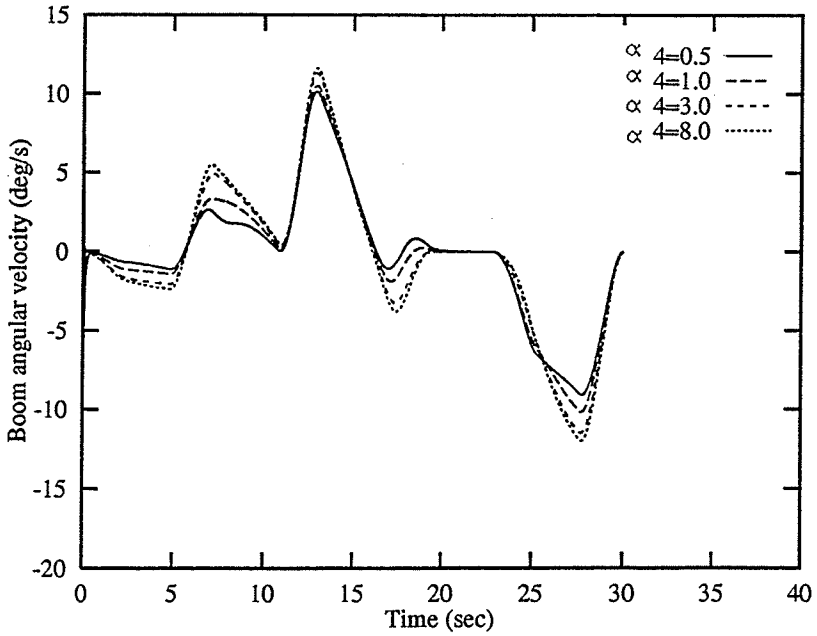

Figure 4.36: Boom angular velocity for different values of α_4.

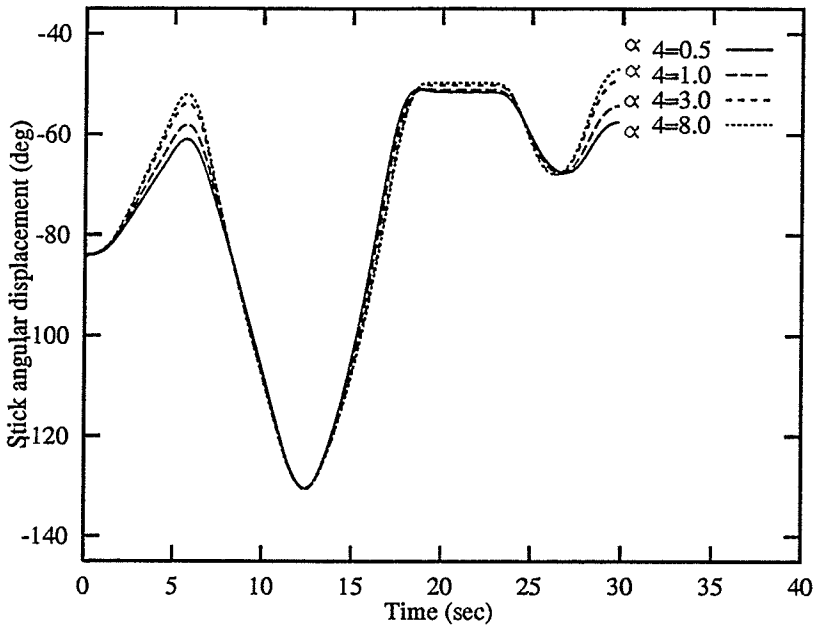

Figure 4.37: Stick displacement for different values of α_4.

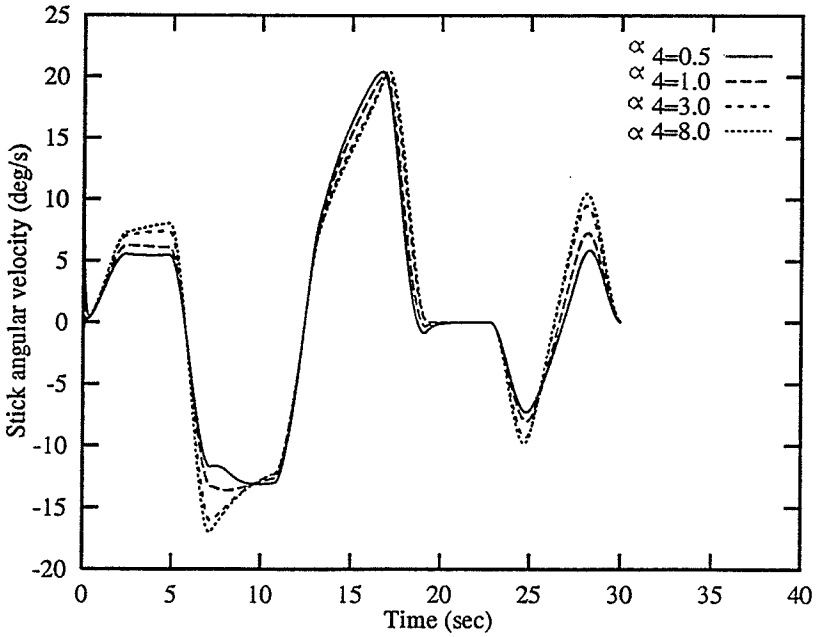

Figure 4.38: Stick angular velocity for different values of α_4.

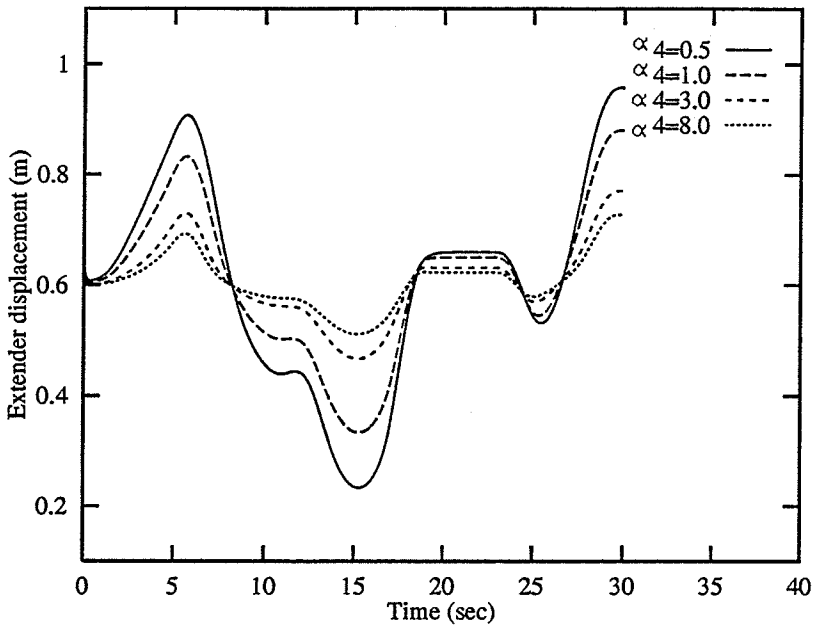

Figure 4.39: Extender displacement for different values of α_4.

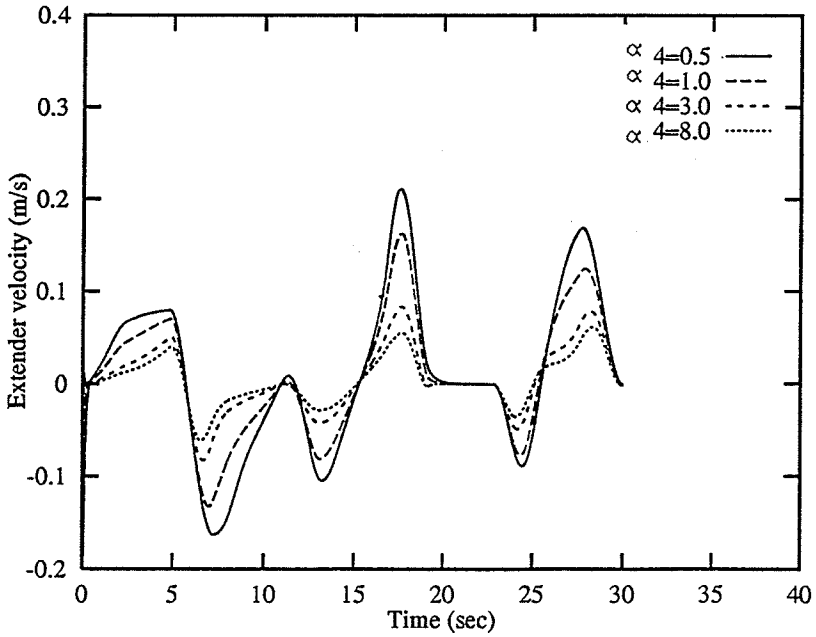

Figure 4.40: Extender velocity for different values of α_4.

large links, thereby increasing the stability of the operation. Furthermore, the mobility of the machine can be introduced in the inverse kinematic solution by giving a very high value to corresponding α_i. This will move the machine only if it is absolutely necessary, for example when the commanded position is outside the normal workspace of the machine. A processor can be introduced in the control loop to aid the operator in selection of appropriate motions.

CHAPTER 5

CONCLUDING REMARKS

Construction, forestry and mining industries utilize heavy-duty manipulator-like machines such as excavators and feller-bunchers. The present operation and control of these machines are very much operator dependent and require significant visual feedback, judgment and skill. This thesis forms part of an investigation which is aiming at enhancing the operation of these machines. One objective is to replace the multi-lever joint control with a single-joystick control. This type of control which is referred to as "coordinated-motion control" has proven to make the operation safer, less stressful and more productive.

A class of these machines contain redundant linkages. Although inverse kinematic solution is trivial for non-redundant manipulators, it may become very complex for redundant manipulators especially when the redundancy is to be efficiently utilized to deal with some particular problems. The focus of this thesis was on the development of a real-time solution to the inverse kinematics of such class of machines during coordinated-motion control.

A new performance criterion was developed which successfully avoided the joints from reaching their limits and at the same time generated smooth joint motions. An efficient gradient projection optimization technique was adopted for numerical solutions. The algorithm proved to be computationally fast and suitable for real-time applications. The scheme also included the machine's power

limitations. Loading and coupled actuation were considered to generate efficient joint motions for the required task.

The joint limit avoidance capability of the scheme was verified using a four degree-of-freedom redundant excavator machine, a Spyder by Kaiser. The suitability of the technique was further validated by comparing the simulation results with the experimental data obtained from an instrumented Caterpillar 215B excavator. While operating in a coordinated-mode, the simulations generated similar joint motions as an experienced operator would generate using a joint-mode control.

The performance criterion developed in this study was also compared with the previously developed criteria. It was shown that the proposed criterion can be configured to produce different levels of smoothness in joint velocity profiles or, joint limit avoidance capability. Previously developed criteria were shown to be special cases of the one developed in this thesis.

Finally, it was discussed that by the appropriate selection of weighting factors introduced in the formulation, any joint can be made more active or sluggish. This allows one to scale the relative movements of individual links to enhance the machine stability or operation workspace. Lighter links can be made more active than the heavier links to reduce the vibrations and to increase the stability of the machine.

Future work may include introducing the machine mobility in the inverse kinematic solution by including the base motion.

REFERENCES

Baillieul, J., 1985. "Kinematic Programming Alternatives for Redundant Manipulators," *Proceedings, IEEE Int. Conference on Robotics and Automation,* St. Louis, MO, pp. 722–728.

Chavez, R.J., and Amazeen, C.A., 1983. "Robotics Applied to Rapid Excavation," *Proceedings, 13th International Symposium on Industrial Robots and Robots 7,* Chicago, Illinois, pp. 94–108.

Cherchas, D.B., and Michalson, R., 1983. "Feasibility Study on the Long Term Application of Robotic Manipulators in Forest Product Operations," *University of British Columbia, Department of Mechanical Engineering, Compute Aided Manufacturing and Robotics Laboratory* (CAMROL),Report No. 83-1.

Dubey, R.V., Euler, J.A., and Babcock, S.M., 1988. "An Efficient Gradient Projection Optimization for the Seven-Degree-of-Freedom Redundant Robot with Spherical Wrist," *Proceedings, IEEE Int. Conference on Robotics and Automation,* Philadelphia, PA, pp. 28–36.

Euler, J.A., Dubey, R.V., and Babcock, S.M., 1988. "Self Motion Determination Based on Joint Velocity Bounds for Redundant Robots," *Proceedings, 2nd Int. Symposium of Robotics and Manufacturing Research, Education, and Application,* Albuquerque, NM.

Fu, K.S., Gonzalez, R.C., Lee, C.S.G., 1987. *Robotics: Control, Sensing, Vision, and Control,* McGraw-Hill, Inc., New York.

Karkkainen, P., and Manninen, M., 1983. *Real-Time Control Method of Large-Scale Manipulators in Robotics,* (B. Rooks ed.), Anchor Press Ltd., Colch-

ester, England, pp. 227–230.

Kazerounian, K., and Wang, Z., 1987. "Global versus Local Optimization in Redundancy Resolution of Robotic Manipulators," *The Int. J. of Robotics Research*, Vol. 7, No. 5, pp. 3–12.

Lawrence, P. D., Sassani, F., Sauder, B., Sepehri, N., Wallersteiner, U. and Wilson, J., 1993. "Computer-Assisted Control of Excavator-based Machines," *Int. Off-Highway and Power Plant Congress*, Milwakee, WI.

Liegeois, A., 1977. "Automatic Supervisory Control of the Configuration and Behavior of Multibody Mechanics," *IEEE Trans. on Systems, Man, and Cybern.*, Vol. SMC-7, No. 12, pp. 868–871.

Nakamura, Y., Hanafusa, H., and Yoshikawa, T., 1987. "Task Priority Based Redundancy Control of Robot Manipulators," *The Int. J. of Robotics Research*, Vol. 6, No. 2, pp. 3–15.

Paul, R., 1981. *Robot Manipulators: Mathematics, Programming and Control*, MIT Press, Cambridge, MA.

Sepehri, N., 1990. *Dynamic Simulation and Control of Teleoperated Heavy-Duty Hydraulic Manipulator,* Ph.D. Thesis, Department of Mechanical Engineering, University of British Columbia.

Sheridan, T.B., 1986. "Human Supervisory Control of Robot Systems," *Proceedings, IEEE Int. Conference on Robotics and Automation*, San Francisco, California, pp. 808–812.

Shirai, Y., 1984. "Key Issues of Robotic Research," *Proceedings, Second Int. Symposium in Robotic Research (H. Hanafusa and I. Hirochica, eds.)*, MIT Press, Cambridge, pp. 505-510.

Vaha, P., and Halme, A., 1984. "Adaptive Digital Control for a Heavy-Duty Manipulator," *Advanced Software in Robotics (A. Danthine and M. Geradin, eds.)*, Elsevier Science Publishers B.V., North Holland, pp. 55–60.

Whitney, D.E., 1972. "The Mathematics of Coordinated Control of Prosthetic Arms and Manipulators," *ASME J. of Dynamic Systems, Measurement, and Control*, Vol. 94, No. 4, pp. 303–309.

Zghal, H., Dubey, R.V., and Euler, J.A., 1990. "An Efficient Gradient Projection Optimization for the Manipulators with Multiple Degrees of Redundancy," *Proceedings, IEEE Int. Conference on Robotics and Automation*, Cincinnati, Ohio, pp. 1006–1011.

APPENDICES

APPENDIX A

KINEMATICS OF KAISER SPYDER

A.1 Homogeneous Transformations

The four-degree-of-freedom Spyder manipulator, shown in Figure 2.1, is assigned four coordinate frames associated with each of the four joints of the manipulator as shown in Figure A.1. Using the Denavit–Hartenberg notation and letting coordinate frame (i) be the frame associated with the i^{th} joint, the position and orientation of frame (i) relative to frame $(i-1)$ can be represented by the homogeneous transformation $\mathbf{A}_i^{i-1}$given by the following (4×4) matrix (Paul 1981):

$$\mathbf{A}_i^{i-1} = \begin{bmatrix} \cos\theta_i & -\sin\theta_i \cos\alpha_i & \sin\theta_i \sin\alpha_i & a_i \cos\theta_i \\ \sin\theta_i & \cos\theta_i \cos\alpha_i & -\cos\theta_i \sin\alpha_i & a_i \sin\theta_i \\ 0 & \sin\alpha_i & \cos\alpha_i & d_i \\ 0 & 0 & 0 & 1 \end{bmatrix} \tag{A.1}$$

where

- a_i is the link length
- α_i is the twist angle
- d_i is the distance between links
- θ_i is the angle between links

The first three columns of $\mathbf{A}_i^{i-1}$ represent the coordinate transformation that specifies the orientation of frame (i) relative to frame $(i-1)$ while the fourth

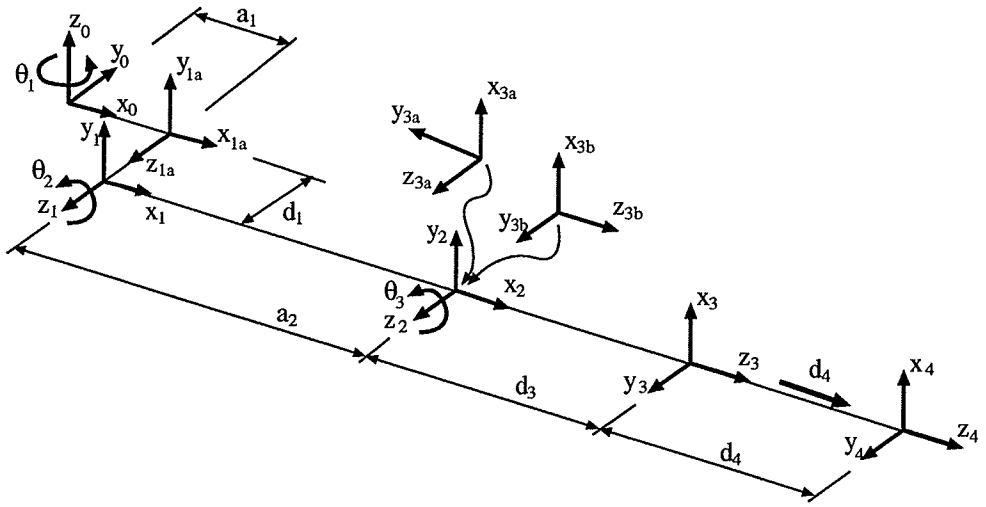

Figure A.1: Manipulator coordinate frames.

Table A.1: Kinematic Parameters for Jacobian of Spyder

joint i	Link	α_i (deg.)	a_i (mm)	d_i (mm)	θ_i (deg.)
1a	Swing-1	90	610	0	θ_1 (Unbounded)
1	Swing-2	0	0	50	0
2	Boom	0	2800	0	θ_2 (-20 to 60)
3a	Stick-1	0	0	0	$90 + \theta_3$ (-145 to -45)
3b	Stick-2	90	0	0	0
3	Stick-3	0	0	1400	0
4	Extender	0	0	d_4 (100 to 1100)	0

column represents the position of frame (i) relative to frame $(i-1)$.

The Denavit–Hartenberg parameters for the coordinate frames associated with all joints are listed in Table A.1. The homogeneous transformations associated with all four joints of the Spyder are determined by substituting the parameters listed in the table into (A.1). An intermediate coordinate frame $(1a)$ is used to account for the fact that link1 is not collinear with the x_0 axis. Two other intermediate coordinate frames $(3a)$ and $(3b)$ are used to properly handle the transition from the revolute joint (3) to the prismatic joint (4). The homogeneous

transformations are given as following:

$$\mathbf{A}_{1a}^{0} = \begin{bmatrix} c_1 & 0 & s_1 & a_1c_1 \\ s_1 & 0 & -c_1 & a_1s_1 \\ 0 & 1 & 0 & 0 \\ 0 & 0 & 0 & 1 \end{bmatrix}, \quad \mathbf{A}_{1}^{1a} = \begin{bmatrix} 1 & 0 & 0 & 0 \\ 0 & 1 & 0 & 0 \\ 0 & 0 & 1 & d_1 \\ 0 & 0 & 0 & 1 \end{bmatrix}$$

$$\mathbf{A}_{1}^{0} = \mathbf{A}_{1a}^{0}\,\mathbf{A}_{1}^{1a} = \begin{bmatrix} c_1 & 0 & s_1 & a_1c_1 + d_1s_1 \\ s_1 & 0 & -c_1 & a_1s_1 - d_1c_1 \\ 0 & 1 & 0 & 0 \\ 0 & 0 & 0 & 1 \end{bmatrix}$$

$$\mathbf{A}_{2}^{1} = \begin{bmatrix} c_2 & -s_2 & 0 & a_2c_2 \\ s_2 & c_2 & 0 & a_2s_2 \\ 0 & 0 & 1 & 0 \\ 0 & 0 & 0 & 1 \end{bmatrix}$$

$$\mathbf{A}_{3a}^{2} = \begin{bmatrix} -s_3 & -c_3 & 0 & 0 \\ c_3 & -s_3 & 0 & 0 \\ 0 & 0 & 1 & 0 \\ 0 & 0 & 0 & 1 \end{bmatrix} \quad \mathbf{A}_{3b}^{3a} = \begin{bmatrix} 1 & 0 & 0 & 0 \\ 0 & 0 & -1 & 0 \\ 0 & 1 & 0 & 0 \\ 0 & 0 & 0 & 1 \end{bmatrix} \quad \mathbf{A}_{3}^{3b} = \begin{bmatrix} 1 & 0 & 0 & 0 \\ 0 & 1 & 0 & 0 \\ 0 & 0 & 1 & d_3 \\ 0 & 0 & 0 & 1 \end{bmatrix}$$

$$\mathbf{A}_{3}^{2} = \mathbf{A}_{3a}^{2}\,\mathbf{A}_{3b}^{3a}\,\mathbf{A}_{3}^{3b} = \begin{bmatrix} -s_3 & 0 & c_3 & a_3c_3 \\ c_3 & 0 & s_3 & a_3s_3 \\ 0 & 1 & 0 & 0 \\ 0 & 0 & 0 & 1 \end{bmatrix}$$

$$\mathbf{A}_{4}^{3} = \begin{bmatrix} 1 & 0 & 0 & 0 \\ 0 & 1 & 0 & 0 \\ 0 & 0 & 1 & d_4 \\ 0 & 0 & 0 & 1 \end{bmatrix}, \tag{A.2}$$

where $c_i = \cos\theta_i$ and $s_i = \sin\theta_i$. $s_{ij} = \sin(\theta_i + \theta_j)$ and $c_{ij} = \cos(\theta_i + \theta_j)$.

A.2 Determination of the Jacobian (Cartesian Coordinates)

The Jacobian relating the joint angular velocities and the end effector velocity of a four-link manipulator with the first three joints being revolute and the last joint being prismatic, can be determined using the vector cross product method (Fu *et al.*, 1987):

$$\mathbf{J}(\Theta) = \begin{bmatrix} \mathbf{z}_0 \times {}^0\mathbf{p}_4 & \mathbf{z}_1 \times {}^1\mathbf{p}_4 & \mathbf{z}_2 \times {}^2\mathbf{p}_4 & \mathbf{z}_3 \end{bmatrix}, \qquad \text{(A.3)}$$

where $\mathbf{z}_{i-1}$ is the unit vector along the axis of rotation or sliding of the i^{th} joint. Vectors $\mathbf{z}_0$, $\mathbf{z}_1$, $\mathbf{z}_2$, and $\mathbf{z}_3$ are given by

$$\mathbf{z}_0 = \begin{bmatrix} 0 \\ 0 \\ 1 \end{bmatrix}, \quad \mathbf{z}_1 = \mathbf{z}_2 = \begin{bmatrix} s_1 \\ -c_1 \\ 0 \end{bmatrix}, \text{and} \quad \mathbf{z}_3 = \begin{bmatrix} c_1 c_{23} \\ s_1 c_{23} \\ s_{23} \end{bmatrix}.$$

The vector ${}^i\mathbf{p}_4$ is the position vector from the origin of the i^{th} coordinate frame to the 4^{th} coordinate frame. The $\times$ symbol denotes the cross product operator. The vectors ${}^0\mathbf{p}_4$, ${}^1\mathbf{p}_4$, and ${}^2\mathbf{p}_4$ are given by

$${}^0\mathbf{p}_4 = \begin{bmatrix} a_1c_1 + d_1s_1 + a_2c_1c_2 + a_3c_1c_{23} + d_4c_1c_{23} \\ a_1s_1 + d_1c_1 + a_2s_1c_2 + a_3s_1c_{23} + d_4s_1c_{23} \\ a_2s_2 + a_3s_{23} + d_4s_{23} \end{bmatrix}$$

$${}^1\mathbf{p}_4 = \begin{bmatrix} a_2c_1c_2 + a_3c_1c_{23} + d_4c_1c_{23} \\ a_2s_1c_2 + a_3s_1c_{23} + d_4s_1c_{23} \\ a_2s_2 + a_3s_{23} + d_4s_{23} \end{bmatrix}$$

$$ {}^{2}\mathbf{p}_4 = \begin{bmatrix} a_3c_1c_{23} + d_4c_1c_{23} \\ a_3s_1c_{23} + d_4s_1c_{23} \\ a_3s_{23} + d_4s_{23} \end{bmatrix} $$

For the four-degree-of-freedom Spyder, the Jacobian of the end-effector translational velocity $\mathbf{J_T}$ is given by

$$ \mathbf{J}_T = \begin{bmatrix} -[a_1s_1 - d_1c_1 + s_1(a_2c_2 + a_3c_{23} + d_4c_{23})] & -c_1(a_2s_2 + a_3s_{23} + d_4s_{23}) & -c_1(a_3s_{23} + d_4s_{23}) & c_1c_{23} \\ a_1c_1 + d_1s_1 + c_1(a_2c_2 + a_3c_{23} + d_4c_{23}) & -s_1(a_2s_2 + a_3s_{23} + d_4s_{23}) & -s_1(a_3s_{23} + d_4s_{23}) & s_1c_{23} \\ 0 & a_2c_2 + a_3c_{23} + d_4c_{23} & a_3c_{23} + d_4c_{23} & s_{23} \end{bmatrix} $$

A.3 Jacobian for Cylindrical Coordinates

In the case when operator is present on the machine the joystick is sampled in cylindrical coordinates. This can be achieved by dividing the workspace into two parts, a vertical plane and rotation of this plane about a vertical axis (see Figure A.2). If 'left/right' motion of the joystick is assigned to the rotation of the machine (θ_1) about a vertical axis, only two variables (R and Z) are left to be controlled in the vertical plane by utilizing the three links boom, stick and extender. The jacobian can then be formulated using only three links. Various coordinate frames are show in Figure A.3. All the steps for finding the jacobian are similar to Section A.2. The jacobian in this case reduces to:

$$ \mathbf{J}_R = \begin{bmatrix} -(a_3 + d_4)s_{23} - a_2s_2 & -(a_3 + d_4)s_{23} & c_{23} \\ -(a_3 + d_4)c_{23} - a_2c_2 & -(a_3 + d_4)c_{23} & s_{23} \end{bmatrix}. $$

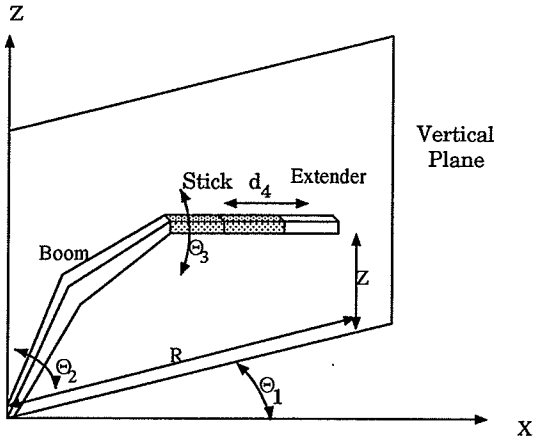

Figure A.2: Manipulator in Cylindrical Coordinates

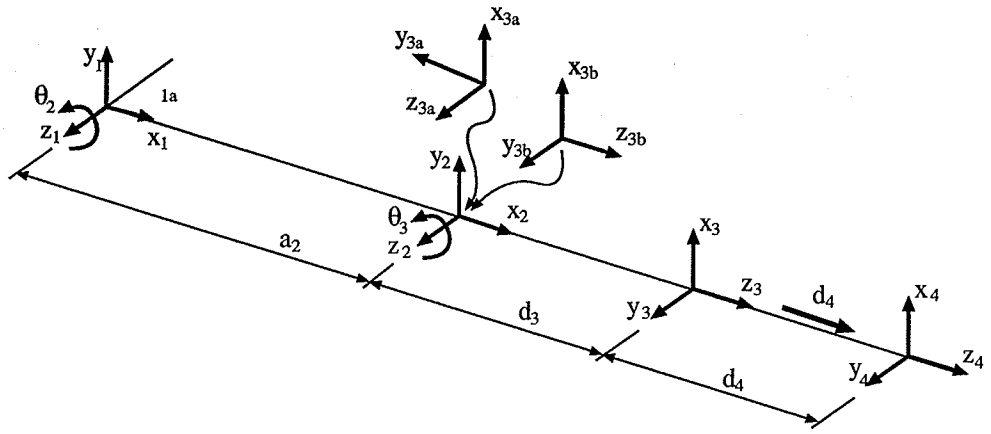

Figure A.3: Manipulator coordinate frames in cylindrical coordinates.

APPENDIX B

COMPARISON OF PERFORMANCE CRITERIA FOR EXPERIMENTAL DATA

In this Section, the new performance criterion is evaluated with respect to the existing criteria for the experimental data (see Section 3.3. All criteria generated deferent joint motions given the same end-effector motion. As mentioned previously the redundancy considered for 215B Caterpillar has no effect on the swing joint motion. Therefore the results for the swing joint are similar for all the cases and hence are not included.

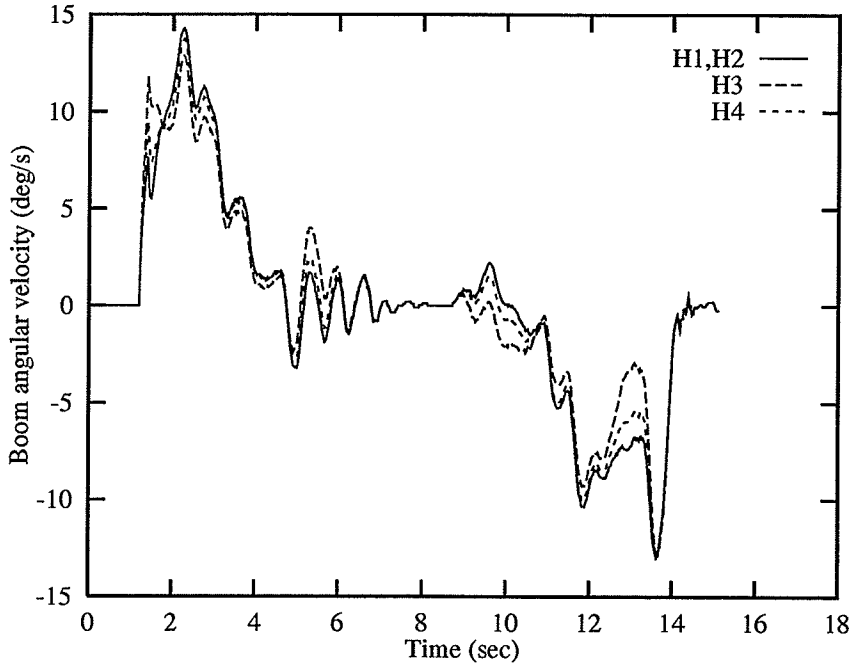

Figure B.1: Boom angular velocity.

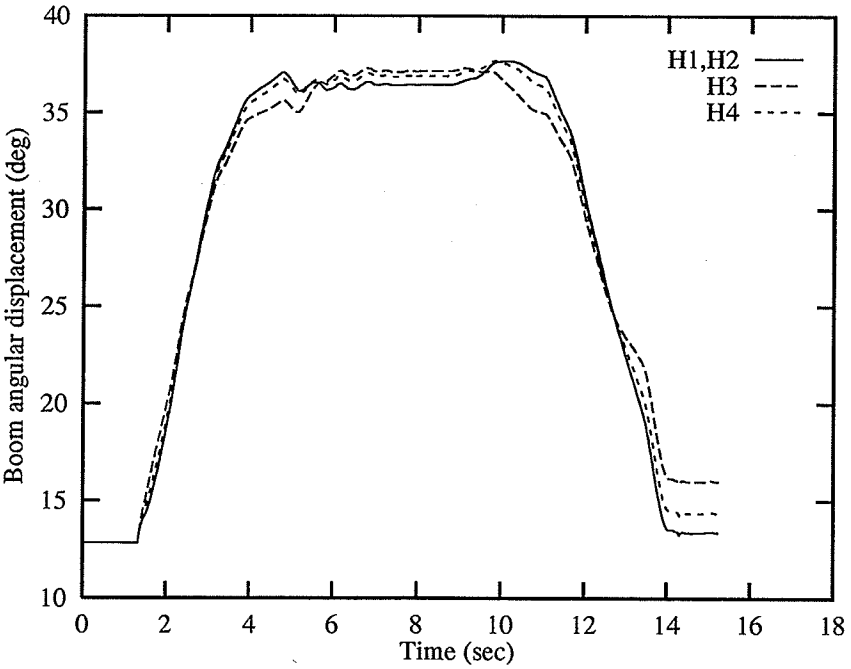

Figure B.2: Boom displacement.

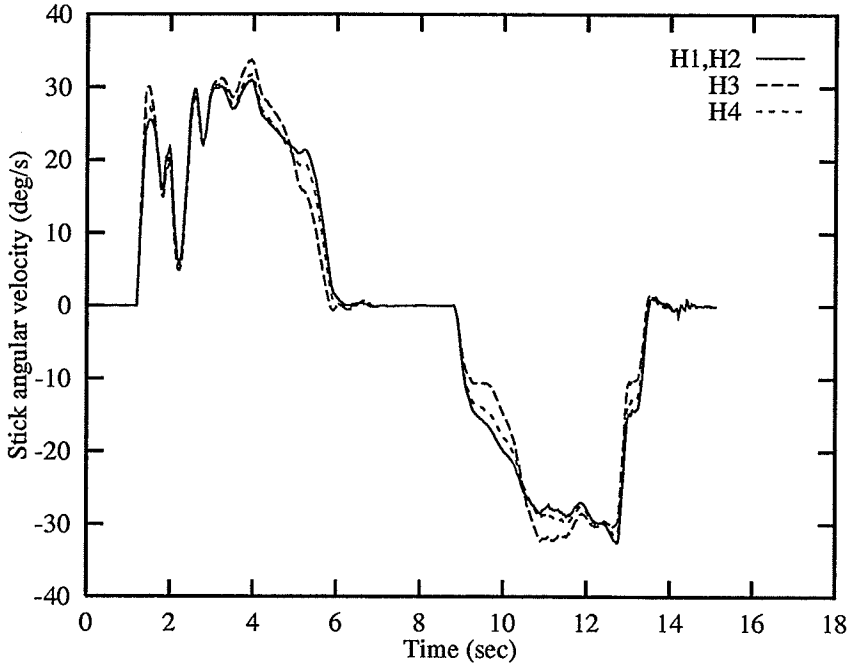

Figure B.3: Stick angular velocity.

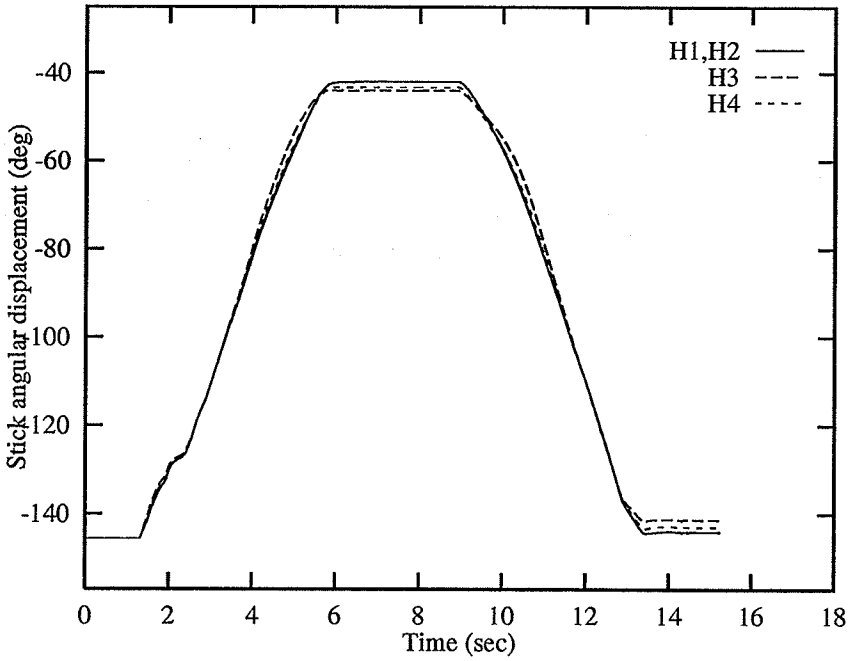

Figure B.4: Stick displacement.

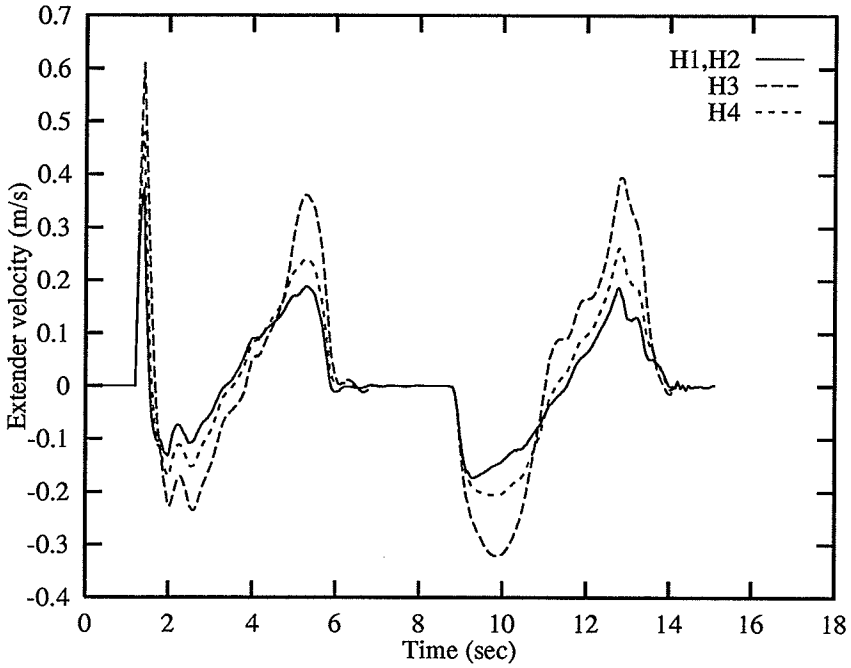

Figure B.5: Extender linear velocity.

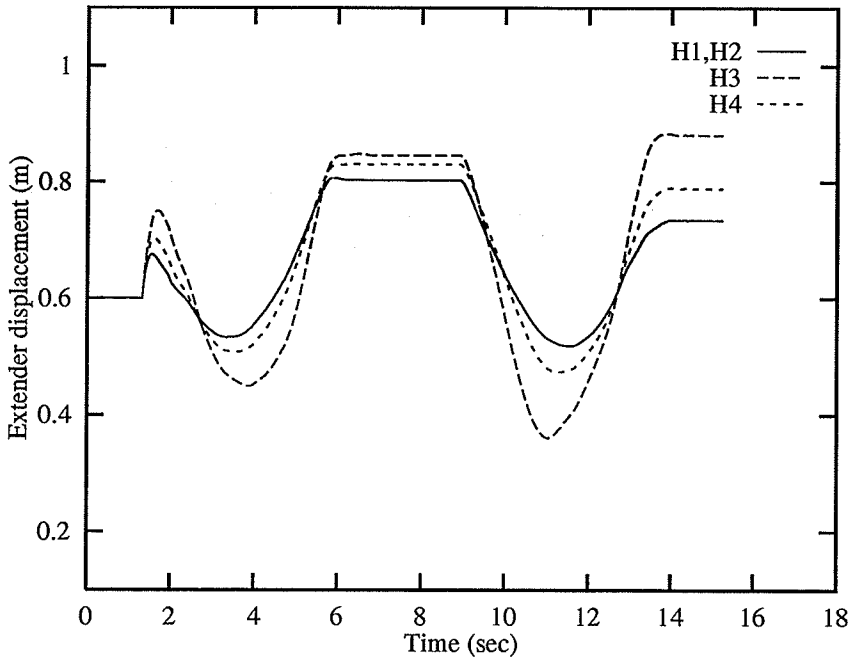

Figure B.6: Extender displacement.